UCID-20731

A General-Purpose, Packed-Bed Model for Analysis of Underground Coal Gasification Processes

Charles B. Thorsness

Sang-Wook Kang

April 25, 1986

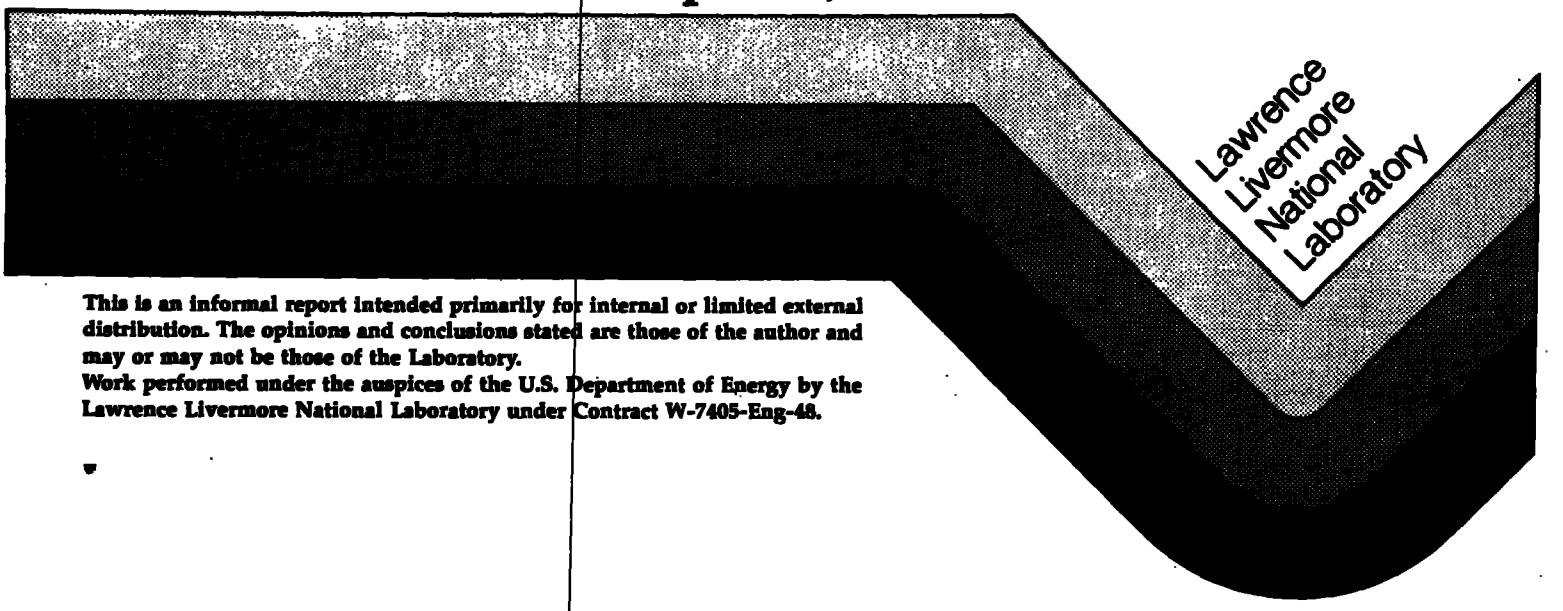

Work performed under the auspices of the U.S. Department of Energy by the Lawrence Livermore National Laboratory under Contract W-7405-Eng-48.

UCID-20731

A General-Purpose, Packed-Bed Model for Analysis of Underground Coal Gasification Processes

Charles B. Thorsness

Sang-Wook Kang

Manuscript Date: April 25, 1986

LAWRENCE LIVERMORE NATIONAL LABORATORY
University of California • Livermore, California • 94550

TABLE OF CONTENTS

LIST OF FIGURES

A GENERAL-PURPOSE, PACKED-BED MODEL FOR ANALYSIS OF UNDERGROUND COAL GASIFICATION PROCESSES*

ABSTRACT

A computer model for characterizing reacting flows through packed beds is presented. These flows are related to the underground coal gasification conditions in terms of combustion and multi-component chemical reactions that take place inside beds of coal char. Time-dependent, two-dimensional (including axisymmetrical) partial differential equations (PDE's) describing conservation of mass, species, momentum, and the thermal energy are formulated. These PDE's are then recast into a set of ordinary differential equations (ODE's) with time as independent variable. The resulting ODE's are solved by applying a method-of-lines (MOL) technique to multi-component flows through packed char beds. The present formulation considers: the transport phenomena at the wall; various transient flow cases; multiple reactions and species; a wide range of options on the boundary conditions: temperature-dependent physical parameters; and rezoning capabilities. A numerical code called GSF has been developed, and computer runs have been performed to verify various aspects of the physical models as well as the numerical approach taken in the present analysis. These include favorable agreements with available analytical solutions for simple, one-dimensional flows and two-dimensional non-isotropic heat transfer to a wall. For more complicated flow situations for which there are no analytical solutions, good agreements have also been obtained between the results of the present method and those of alternative numerical methods.

The code has been applied to several physical situations bearing on the underground coal gasification processes, i.e., wall drying, wall regression during gasification, and water injection into a gasifying bed. Preliminary results demonstrate that the present numerical modeling approach shows promise as a first step in describing the transient thermophysical phenomena taking place inside packed beds.

****

I. INTRODUCTION

The impetus for this work stems from the desire to better understand the underground coal gasification processes. Since a significant portion of the processes takes place inside a packed bed, our motivation is to develop a mathematical/computer model to analyze the physics of the flow phenomena in general, and to determine in particular how such parameters as gas composition and coal consumption are influenced by changes occurring in this stage of the underground system. The present model is intended also to be applicable to the wall-growth problem to help identify dominant physical factors during interaction between the virgin coal in the wall and the cavity rubble bed. Detailed descriptions of the wall-growth process will be useful in interpreting the data to be obtained from our proposed large, laboratory-scale experiments (one-fifth field scale).

A major physical process occurring inside a packed-bed is interaction between flowing gas and solid particles constitutes. Several transport phenomena are involved in this interaction; (1) the gas-phase reactants move to the particle surfaces, react with them, the resultant products then move back into the gas stream; (2) purely gas-phase reactions may occur when combustible gas comes in contact with injected oxygen; (3) heat energy within the bed moves from hotter zones to cooler ones (e.g., from combustion zones to wall areas).

Literature survey reveals that much past work on packed-bed flow dealt mainly with some specific aspects of the problem. While this enabled them to make simplifying assumptions, often affording them very economic solution schemes, it also limited their adaptability to more generalized models. For example, past packed-bed models, such as those of Thorsness et al.(1978) and of Gunn and Whitman (1976), treat one dimensional, steady flow, and are not readily extendable to transient, two dimensional situations. One dimensional, transient case has been treated by Johnson and Hindmarsh (1983), whose results gave good agreement with the quasi-steady model results for oil-shale problems, in some cases even reducing the computation times. As for the gasification processes, the surface phenomena have been investigated by Denn et al.(1982).

Their model is primarily for a steady-state operation and does not consider truly time-dependent, two-dimensional gas flow. However, their basic scheme of dealing with the heterogeneous gas-solid reactions is appropriate for our purposes, and we will adopt that aspect of their method in our present model.

Our approach in characterizing the various physico-chemical processes taking place inside packed beds is to develop a single, generalized mathematical/computer model. The advantages of a single model are; (1) it does not have to introduce simplifying assumptions to address a variety of questions; and (2) it can serve as a test bed for introducing approximations to be used by more comprehensive models. The mathematical model should be based on a fundamental description of the processes occurring in packed beds, especially the ability to describe the solid-phase motion. The proposed model also should be capable of handling various time scales associated with important phenomena, including ignition, changes in injection composition, tracer injection, and burnout of the bed.

With these considerations, a preliminary mathematical/computer model was developed by Thorsness and Kang (1984), and yielded promising results. In the present report, we describe further work performed on the model, including model improvements and partial verification runs. In particular, we have made improvements in the following areas: better wall transport model, axisymmetric geometry, more reactions and species (8 reactions, up to 7 species), more options on boundary conditions, rezoning capability, injection of fluid or heat anywhere in the bed, and temperature-dependent physical parameters.

Details of these new developments are given in subsequent sections. Conservation equations, various chemical reactions, transport properties, and boundary conditions are given in Section II, followed by the method of solution in Section III, in which we also include the computer size and time considerations. Verification of many aspects of the numerical code is discussed in Section IV. Application of the present model to several situations related to the underground coal gasification processes is presented in Section V.

II. FORMULATION

In formulating packed-bed flows we make the following assumptions and conditions. Though seemingly self-explanatory, rationale for these assumptions will be discussed in the text where necessary.

Assumptions.

1. Temperature: Equal gas and solid temperatures at a given point in space;
2. Species: Two solid species (carbon and ash) and seven gas species (nitrogen, oxygen, hydrogen, carbon monoxide, carbon dioxide, water vapor, and methane);
3. Geometry: One or two-dimensional (including axisymmetric);
4. Gas phase: Ideal gas law;
5. Gas phase: Darcy's law;
6. Solid phase: Three cases are analyzed:
   (a) the solids are stationary;
   (b) the solid velocity is prescribed at a constant value in the vertical direction, and zero in the horizontal direction;
   (c) a simple bed-settling model, taking the overall-bed density to be constant and the solids moving straight downward.
7. Heterogeneous reactions: For the solid-particle-gas reactions, two kinetic models are used, based on Yoon, et al (1978). These are AS and SP models, the term AS denoting "ash segregation" while SP signifies "shell progressive", respectively. More on this later.
8. Ash: Fixed ash particle size (at some fraction of the original particle size).
9. Wall region: In the wall region, a thin region exists through which thermal energy is exchanged such that a conventional heat transfer coefficient adequately characterizes the transport phenomena; (Details will be given in the section on the boundary conditions.)

Any additional features will be specified and discussed in the text as they occur.

The above model is a compromise between completeness and expediency. We wanted enough complexity to permit evaluation of the usefulness of the current approach without expending an undue amount of time developing detailed model physics. For example, although the current model employs only two solid and seven gas species, the extension to more gas species is conceptually simple, requiring only a definition of reaction kinetics for the component. In contrast, extension of the present formulation to more solid species is somewhat more complicated.

Based on the above set of conditions, the following mass and energy conservation relationships are derived for the solid and the gas phases.

Gas-phase mass balance.

Overall gas conservation :

$$\frac{\partial(\phi C)}{\partial t} = -\nabla\cdot(\vec{v}\phi C) + \sum_{i=1}^{n} Q_i + \sum_{i=1}^{n} s_i \qquad (1)$$

where the term C denotes total gas concentration in mol/m^3 of gas-filled porosity, ϕ the total bed porosity, t the time in seconds, v the "effective" gas velocity in m/s, Q_i the rate of introduction of gas species i into the bed, s_i the source rate of gas species i per unit volume of bed in mol/m^3-s, subscript i an index for gas species, and n the number of gas species. A definition of all variables is listed at the end of the report in the Nomenclature section.

The effective gas velocity (v) is related to the superficial and interstitial velocities in the following way. The superficial velocity (U) is a convenient term describing an average velocity with which the gas flows through the total cross-sectional area of the bed. In the present formulation we consider porosity both internal and external to the solid particles. The superficial gas velocity is then the product of the total bed porosity and the effective

gas velocity (v). On the other hand, the interstitial gas velocity (v_{int}) is physically a more realistic property and signifies the velocity with which the gas flows through a local void area (Sherwood, Pigford, and Wilke 1975). In mathematical form these relationships are : $U = \phi_e v_{int} = \phi\ v$

Conservation of Gas species :

$$\frac{\partial(\phi c_i)}{\partial t} = -\nabla\cdot(\vec{v}\phi c_i) + Q_i + s_i + \nabla\cdot(CD\nabla y_i) \qquad (2)$$

where c_i denotes concentration of gas species i in mol/m^3 of gas-filled porosity, D effective mass dispersion in bed in m^2/s, y_i mole fraction of gas species i.

Mass Balances (Solid-phase) .
Overall solid conservation :

$$\frac{\partial[(1-\phi)\rho_s]}{\partial t} = -\nabla\cdot[(1-\phi)\rho_s\vec{v}_s] + \sum_{k=1}^{k=m} s_k^* \qquad (3)$$

where ρ_s denotes average density of solid particle in kg/m^3, v_s true solid velocity in m/s, s_k^* production rate for solid species k per unit volume of bed in kg/m^3-s, subscript k an index for solid species, and m the number of solid species. Currently we are using two solid species, i.e., carbon and ash.

Solid species conservation :

$$\frac{\partial[(1-\phi_e)\rho_s w_k]}{\partial t} = -\nabla\cdot[(1-\phi_e)\rho_s w_k\vec{v}_s] + s_k^* \qquad (4)$$

where w_k signifies mass fraction of solid species.

The overall equation is simply the sum of the individual species-conservation equations. It is included here, however, because we use these relationships to calculate the gas- and solid-phase velocities.

Conservation of Energy .

The energy balance for the entire system, in which we invoke the assumption of identical gas and solid temperature (Assumption 1), is given by the following equation

$$\frac{\partial[\phi\sum_{i=1}^{n}(c_i h_i) + (1-\phi_o)\rho_s\sum_{k=1}^{m}(w_k h_k^*)]}{\partial t} =$$

$$-\nabla\cdot[\sum_{i=1}^{n}(h_i\vec{j}_i)] - \nabla\cdot[\rho_s\nabla_s\sum_{k=1}^{m}(w_k h_k^*)] + W + \nabla\cdot(k\nabla T) \qquad (5)$$

where h_i denotes enthalpy of gas species i in J/mol, j_i total flux of gas species i in mol/m^2-s and is given by

$$j_i = v\phi c_i - D\ C\ \nabla y_i$$

The symbol k in Eq.(5) signifies the effective thermal conductivity in the bed in W/m-k, T the temperature in K, W the rate of heat introduced into the bed, and h_k^* the enthalpy of solid species k in J/kg.

Equation of State .

In line with the ideal gas assumption, we have

$$P = C\ R\ T \qquad (6)$$

where the term r signifies the static pressure in Pa, R the gas constant for the gas mixture in J/mol-K (or Pa-m^3/mol-K), and C the total gas concentration in mol/m^3.

In Eqs.(1)-(6), there are 10 + i + k dependent variables, i.e., C, v, c_i, y_i, U, v_s, w_k, h_i, h_k^*, T, and P. Of these, the static enthalpy term h_i is a function of T and c_i, while the static enthalpy term for solid phase (h_k^*) is a function of T and w_k. Also, the velocity terms U and v are related by $v = U/\phi$, y_i and c_i are related by $y_i = c_i/C$, thus reducing the number of unknowns to seven. We therefore need an additional equation to completely define the flow characteristics. This is accomplished by relating v and P invoking Darcy's law (Assumption 5) - see Eq. (7).

Once these dependent variables are calculated from solution of the partial differential equations, other parameter values, such as the porosity, can be determined from relevant relationships previously derived (Thorsness and Kang 1984). We now give details of these steps.

Gas motions.

In the present formulation we do not explicitly use the overall mass balance equations for both the gas and solid phases; instead we expand the equations to derive expressions for gas and solid velocities. Currently only crude models are employed. In line with the Assumption 5, we invoke Darcy's law in the gas phase, i.e., velocity and pressure in the bed are related by

$$\vec{U} = -(\Gamma/\mu)\nabla P \tag{7}$$

where the term Γ signifies permeability in m^2 and μ the average gas viscosity in Pa-sec. When this equation is substituted in Eq. (1), the gas velocities can be eliminated from the equation. After substitution and by using the ideal-gas law, the equation can either be viewed as an equation for pressure, P, or bed-gas distribution, ϕC. In order to maintain a conservative formulation we choose to view the equation as one for ϕC and then by use of appropriate back substitution the gas velocity can be obtained.

Solid-phase motions.

Concerning the flow physics of the solid phase, we conceptualize three situations (Assumption 6). The first situation considered is the absence of any solid motions, that is, $v_s = 0$. For this case, Eq.(3) for the overall solid is not required and therefore it is not used.

In the second situation we envision a uniform flow of the solids in one direction, and we set the solid velocity at a constant value in the bulk flow direction and at zero in the horizontal direction, i.e.,

v_s = constant (y-direction), and
$v_s = 0$ (x-direction).

This second case is a rather simple way of simulating the solid-phase motions.

The third situation represents our first attempt at characterizing the solid-settling behavior in packed beds in a more general manner. Here we assume that the overall bed density remains constant and that the solids only move in a straight downward direction, i.e., $(1-\phi_e)\rho_s$ = constant. This removes the transient term from Eq. (3) and allows the equation to be integrated in the vertical direction, yielding the solid velocity as a function of position and time

$$v_s(y,t) = v_{s0} + \frac{1}{\rho_s}\int_{y=0}^{y} s_c^*(y,t)\,dy \qquad (8)$$

where the term v_{s0} denotes the solid particle velocity at the bed bottom in m/s, the subscript c the char, y the coordinate in the bulk-flow or vertical direction in meters.

Heterogeneous Reactions -- AS and SP Models

In order to solve the system of differential equations (1) -(5), we need to derive expressions for the production rates s_i and s_k^*, characterizing solid- gas interactions. For this purpose the kinetic model described in Assumption 7 has been employed in the present analysis. The model represents an extension of the models employed by Yoon et al (1978). Two basic kinetic models have been derived for the heterogeneous reactions encompassing two extremely opposite behaviors. For both models, a single initial particle size (monodisperse) is treated; however, extension to a more general case of various initial-size distributions is possible. The models assume that the apparent rate of an individual reaction may be controlled by: (i) gas-film diffusion external to the particle, (ii) diffusion through an ash layer, (iii) diffusion into the reacting particle, or (iv) intrinsic surface reaction rate. We now discuss details of these two models.

In the Shell Progressive (SP) model, it is assumed that a core of unreacted solid is surrounded by a shell of ash. For the gas phase reactants to reach the unreacted core they must not only diffuse through the external gas film but also through this ash layer. On the other hand, the Ash Segregation (AS) model assumes that the ash falls away from the particle leaving unreacted material exposed to the gas stream.

Consideration of both AS and SP models for the present problem is useful because these two models should represent extremes in possible behavior. This fact then enables us to bracket the magnitudes of the relevant reactions taking place in the bed.

In both of these models the particle diameter plays a prominent role, and the particle sizes used in the correlations are assumed to be a function of position in the bed and amount of reaction which has occurred. Therefore at any one time there is a distribution of particle sizes in the bed. In the SP model there is a minimum size the particle can attain during heterogeneous reactions bacause of the ever-thickening ash layer surrounding the particle as the fraction of unreacted char goes to zero. This minimum size depends on initial particle size and ash concentration. By contrast, for the AS model the diameter for the unreacted solid particle can reach zero (because now there is no ash layer tending to inhibit reactions at the surface), along with the ash particles whose size is taken to be a certain fraction of the initial particle size (25% is used here -- see Assumption 8). Additional discussions and relations for particle size and other terms derived for these models are given later in this section as well as in Appendix A.

Reaction rates.

In characterizing the reaction activities taking place between the gas and the solid in packed-beds, we have used seven chemical reactions in the present analysis. Four of these are concerned with the heterogeneous reactions, i.e., carbon and other species. The fifth reaction, water-gas-shift (WGS), is quasi-heterogeneous in that the gas-phase species involved in this reaction are highly catalyzed by the presence of solid surfaces, such as happens in packed beds. The remaining three reactions considered here describe purely gas-phase reactions.

Heterogeneous reactions.

There are four heterogeneous reactions for both AS and SP modles. These are:

Reaction 1: $C + 1/2\ O_2 \rightarrow a\ CO + (1 - a)\ CO_2$

Reaction 2: $C + CO_2 \leftrightarrow 2\ CO$

Reaction 3: $C + H_2O \leftrightarrow CO + H_2$

Reaction 4: $C + 2\ H_2 \leftrightarrow CH_4$

For the SP model the reaction rates are given in the form, adapted from Yoon, et al (1978);

$$r_{SP} = \frac{\pi N (c - c_{eq})}{\frac{1}{k_c d_p^2} + \frac{1-F}{2D_e d_p} + \frac{6}{\eta k_r \rho_c d_u^3}} \qquad (9)$$

where the term r is the reaction rate per volume of bed in mol/m^3-sec, N number of solid particles per volume of bed in particles/m^3, $c - c_{eq}$ the concentration potential for reaction, k_c the gas-film mass transfer coefficient in m^2/s, d_p particle diameter in m, F the fraction of the particle diameter which is occupied by unreacted core, D_e effective gas diffusivity inside a particle in m^2/s, η reaction effectiveness factor, k_r intrinsic reaction constant in 1/s, ρ_c carbon density in unreacted solid in kg/m^3, and d_u the unreacted particle diameter in m. Physically, the first term in the denominator in Eq. (9) signifies the bulk mass transfer of reactants to the particle surface, the second term the diffusion through the ash layer, and the third term the diffusion into and the intrinsic reactions at the surfaces of the unreacted core. The reactions are thus limited by these three mechanisms for a particle in SP reaction model.

With the AS model there is no ash layer and the reaction rate is given by

$$r_{AS} = \frac{\pi N (c - c_{eq})}{\frac{1}{1 - k_c d_p^2} + \frac{6}{\eta k_r \rho_c d_p^3}} \qquad (10)$$

and is dependent on only two coupled mechanisms, bulk mass transfer of reactants to the particle surface and diffusion and reaction in the unreacted particle.

Water-gas-shift reaction. In addition to the above heterogeneous reactions we add the WGS reaction

Reaction 5: $CO + H_2O \rightarrow CO_2 + H_2$

Even though it involves only gas phase species, it is highly catalyzed by solid surfaces and as a result nearly all the reaction occurs on surfaces in a packed bed situation. For this reaction the same basic form as those given above are used, except that in the SP model the particles are taken to be uniformly active calalysts (i.e., no unreacted core is considered) and the rate is given by the AS model expression modified with appropriate particle diameters. On the other hand, the rates for AS model should account for the presence of both the unreacted particles and the ash particles. Therefore, we take the overall rate to be the sum of two rates, one using the unreacted particle parameters in the AS expression and one using the ash particle parameters.

Intrinsic reactions. In both AS and SP models it has been assumed that the intrinsic reaction rate of carbon and gas can be adequately represented by the simple form

$$r^* = A\,(c - c_{eq})\,\exp\,(-E/RT) \qquad (11)$$

where the primary gas phase reacted is included here in a simple first order manner, and c_{eq} the equilibrium concentration expressed in terms of other properties. For example, for the reaction 5 just described, we have :

$$c_{eq} = (c_3 c_5)/(0.0265 c_6)\exp(-3920/T).$$

Other reactions possess similar expressions.

The expression for the intrinsic rate of the water-gas-shift is somewhat more complicated. It is taken from Govind and Shah (1984)

$$r_s = 568RT\,(0.5-\frac{P\times10^{-7}}{2.53})([CO]-[CO]_{eq})\,\exp\,(-13971/T) \qquad (12)$$

The k_r used for this case in the overall rate expression includes everything except the carbon monoxide concentration.

Purely gas-phase reactions.

We now consider three, strictly gas-phase reactions, which are included to allow gas-phase combustion. The reactions selected are

Reaction 6: $CO + 1/2\ O_2 \rightarrow CO_2$

Reaction 7: $H_2 + 1/2\ O_2 \rightarrow H_2O$

Reaction 8: $CH_4 + 2\ O_2 \rightarrow CO_2 + 2\ H_2O$

The rates for the reactions 6 through 8 can be expressed by the following form:

$$r_j = \frac{\phi_e\, c_2\, A_j\, B_j\, Z_j \exp(-E_j/RT)}{1 + c_2\, A_j\, B_j\, R_s \exp(-E_j/RT)} \qquad (13)$$

wherein the term R_s, representing mass-transfer effects, was added to the reaction rate not so much for physical reasons but as a simple way of limiting gas-phase reaction rates at high temperatures. This aspect will be discussed further in the section on the method of solution.

For CO combustion (reaction 6), we have, from Field et al.(1967):

$A_6 = 4.75\ (10^5)$; $B_6 = 17.5\ c_6^{0.5}\ C^{0.3}/(C+24.7c_6)$;

$Z_6 = c_4\ R_{fact}(6)$; $E_6/R = 8050$ K.

For hydrogen combustion (reaction 7) is given by Peters (1979):

$A_7 = 1.08\ (10^{10})$; $B_7 = 1$;

$Z_7 = c_3\ R_{fact}(7)$; $E_7/R = 15150$ K.

Finally, for methane combustion (reaction 8) is, from Sohrab et al. (1984):

$A_8 = 4.33\ (10^4)$; $B_8 = 1$;

$Z_8 = c_7\ R_{fact}(8)$; $E_8/R = 23{,}200$ K.

Transport properties.

In the partial differential equations, Eqs.(1)-(5), many physical and transport properties are involved in describing packed-bed flows. We now express them in terms of appropriate thermodynamic and flow paramters, such as temperature and the flow velocity.

In particular, four physical properties, i.e., the absolute fluid viscosity, the specific heat of the gas, the heat capacity of the solid, and the thermal conductivity of the solid, are expressed in the model as a linear function of temperature. Details are given in Appendix B. In addition, for the conditions of present interest, we obtain reasonably constant values (0.6) for the Prandtl and the Schmidt numbers. Therefore, using known values of the gas viscosity and specific heat, Prandtl number, and Schmidt number, we can calculate the magnitudes of the diffusivity and thermal conductivity for the gas phase. An extension of property dependence on composition is straightforward but not included in the current model.

In addition, we need expressions for the effective mass and thermal dispersion coefficients in both the axial and the radial directions because the gas species have to flow through the void spaces between the solid particles in packed-bed flows. Much work has been done on determination of these dispersion characteristics (e.g., Coberly and Marshall 1951, Yagi and Kunii 1957, Bischoff and Levenspiel 1962, Edwards and Richardson 1968, Olbrich and

Potter 1972, Schlunder 1978, Dixon and Cresswell 1979, and Wakao and Kaguei 1982). For present purposes we choose the following four correlations to represent these dispersion properties :

Effective Mass Dispersion - Perpendicular (Bischoff 1969);

$$D_p^{eff}/D_g = 0.73\,\phi_e + 0.1\ Re\ Sc \qquad (14)$$

Effective Mass Dispersion - Flow (Edwards and Richardson 1968);

$$D_f^{eff}/D_g = 0.73\,\phi_e + 0.5\ (Re\ Sc)^2/(9.7\,\phi_e + Re\ Sc) \qquad (15)$$

Effective Thermal Transport - Perpendicular (Wakao and Kaguei 1982);

$$k_p^{eff}/k_g = k^0/k_g + 0.1\ Re\ Pr \qquad (16)$$

Effective Thermal Transport - Flow (Wakao and Kaguei 1982).

$$k_f^{eff}/k_g = k^0/k_g + 0.5\ Re\ Pr \qquad (17)$$

where the symbol Pr denotes the Prandtl number, i.e., $Pr = \mu c_g/k_g$, k_g the gas thermal conductivity, Re the Reynolds number based upon the superficial velocity (U) and the particle diameter (d_p), i.e., $Re = Ud_p\rho/\mu$, SC the Schmidt number defined to be $Sc = \mu/\rho\ D_g$, and the subscript f refers to the local flow direction and p the direction perpendicular to the flow. In the model we assume that these compenents can be mapped onto the required x and y directions by constructing an elliptical variation of magnitudes between f and p components. At high temperatures the effective thermal conductivity becomes much greater than the physical thermal conductivity, principally because of the radiative effects becoming dominant at high temperatures, typically above 1300 K. Details are given in Appendix B.

Boundary conditions .

Since there are many situations which we want to study, we list various boundary conditions, along with options to apply relevant conditions to each problem of interest.

For solids, we consider three situations, consistent with Assumption 6. These are : stationary solids, constant solid velocity, and the solid velocity determined from Eq.(8), based on the constant-bed assumption. Thus, all we need to prescribe for the solid motions is either the flux or the velocity of the solids being injected at the exit plane counter to the gas flow direction.

For other dependent variables, such as the species and temperature, the boundary conditions are more complicated, and we list them at four boundaries encompassing the packed-bed flow field, i.e., the inlet plane, the exit plane, the centerline axis, and the wall region (see Figure 1).

(a). Inlet Plane . For species, we prescribe flux values here.

$$f_i = j_i \tag{18}$$

Details are given in Appendix C.
For thermal balances, we impose the condition

$$\left(\sum_{i=1}^{n} f_i h_i\right)_{y=0^-} = \left(\sum_{i=1}^{n} j_i h_i\right)_{y=0^+} - \left(k \partial T/\partial y\right)_{y=0^+} \tag{19}$$

In this equation, the injection temperature and flow are known (prescribed), while the temperature at the inlet position and its gradient are to be obtained as part of the solution. For situations where the temperature gradient is zero at the inlet plane, the equation degenerates to specifying the inlet temperature equal to the temperature at the bed bottom. If solids leave the bottom, we assume that they leave at temperature T(x,0).

(b). Exit Plane. For species at the outflow plane, we impose the zero-gradient condition

$$dc_i/dy = 0 \tag{20}$$

For the energy-balance, we have a radiant heat-exchange capability with the surroundings. Thus we have :

$$-k\, \partial T/\partial y = S\,(T^4 - T_\infty^4) \tag{21}$$

where the term S signifies the product of the emissivity, the Stefan-Boltzmann coefficient, and the "shape factor" (or "viewing factor"). For cases where radiation is assumed zero, this degenerates into a zero-gradient condition.

(c). Centerline. For all dependent variables, that is, both the species and the temperature, we impose axisymmetric condition, i.e., zero gradient:

$$dF/dx = 0 \qquad (22)$$

where F is any dependent variable.

(d). Wall Region. The wall region is defined to be both the vertical wall and the portion of the bottom plane which has no inlet flow. To accommodate various thermal and chemical interactions at the wall boundary, we introduce many optional boundary conditions, including wall-regression due to char formation.

For species, we introduce two possible situations:

(i). No flux at the wall.

$$dy_i/dz = 0 \qquad (23)$$

Here z is the appropriate dimension perpendicular to the wall.

(ii). Finite species flux related to the heat-transfer characterisitcs and the wall drying/pyrolysis model. (This submodel is described in Appendix C.)

For thermal energy balances in the wall region, we have :

(i). Adiabatic wall.

$$dT/dz = 0 \qquad (24)$$

(ii). Heat exhange with the flow through heat-transfer coefficient

a. Isothermal wall temperature, i.e., infinitely large heat-transfer coefficient based on the Nusselt correlation.

b. Variable wall temperature, with either prescribed magnitude for the heat-transfer coefficient, or a built-in correlation for heat transfer between the flowing medium and the wall region.(See Appendix D.)

We note that the last boundary condition can also accommodate the case of wall-regression, for which the grid-dimension rezoning will be made as needed in performing numerical computations. These conditions can be specified independently for the side and the bottom walls with some restrictions.

Effects of AS and SP models.

Before proceeding to discuss the method of solution, it is instructive to compare the relative magnitudes of the various factors that constitute the packed-bed flow phenomena, particularly the particle sizes and the reaction rates. Here we present some typical behavior related to the rate expressions described above. These sample cases are for the conditions of ρ_s = 1000 kg/m^3, ϕ_e = 0.5, f = 0.25, d_0 = 0.025 m, G = 1.0 mol/m^2-s, α = 1.0, and constant bed density. Figure 2 shows the effect of temperature on various reaction rates used for F=1 (full char, no ash) for which case the rates are the same for both SP and AS models, from Eqs.(9) and (10). At low temperatures the rates are dominated almost entirely by intrinsic kinetics (reaction limited) and display sharp decrease with decreasing temperature. At high temperatures, on the other hand, the rates become dominated by internal particle diffusion and finally by external mass flux transported to the particle surface. This general behavior applies to all reactions shown in Figure 2, except for the CO + O_2 reaction. This particular reaction takes place only in the gas phase under the given conditions and consequently is not affected by mass transfer considerations.

As the packed-bed reactions proceed, the fraction of carbon decreases, causing the particle sizes to become smaller and the particle number densities (number of particles per cubic meters) to become large. Here we are making the constant bed density assumption. The quantitative variations of these properties are also given in mathematical form in Eqs.(A.1) through (A.14) in Appendix A. Here we show these in graphic form (Figures 3 and 4) for both SP and AS models. It can be seen from the figures that the particle diameter decreases only slightly and reaches a finite value as the fraction of carbon reaches zero for the SP model, whereas for the AS model the particle size steadily decreases and ultimately goes to zero, consistent with the model assumed. For the AS model, ash particles are generated as the carbon

particles undergo various reactions in the bed. The size of the ash particles is assumed fixed at 25 % of the initial size, i.e., f = 0.25, and thus is 0.00625 m (see Figure 3). As particle sizes diminish with decrease in the carbon fraction in the bed, the number of these carbon particles per unit volume (number density) increases, to satisfy the mass-conservation condition. This is shown in Figure 4, where the number density for unreacted carbon particle (N) is the same for both models and the ash particle number density increases dramatically as its size approaches zero. The mathematical description of this behavior is given in Eqs.(A.13) and (A.14).

The choice of either SP or AS model determines the reaction patterns taking place inside a packed bed as the fraction of carbon diminishes. Figure 5 shows that the carbon oxidation rates decreases sharply with decreasing carbon fraction for SP model, while those for AS model change only slightly for a sizable range of carbon fraction and even display a moderate increase before finally going to zero. This difference in rates is a result of the difference in disposition of the ash in the two models. In the AS model the ash falls away leaving the surface directly accessible to the gas phase, whereas in the SP model an ash layer surrounds the carbon surface, inhibiting reaction with the oxygen there.

The effects of SP and AS models on the water-gas-shift reaction rates are shown in Figure 6 as a function of carbon fraction. Only moderate change is seen for the SP model, in contrast to that for the AS model. Physically, the reason for such a variance between the two models is due to the difference in available surface areas acting as catalyst for the WGS reaction. In the present work, the WGS reaction is the only one affected by the presence of surface areas. For other reactions, only pure (intrinsic) kinetic reactions prevail, such as those involving carbon with CO_2 and H_2O (Reactions 2 and 3 in Figure 2); the surface areas do not act as catalyst for these reactions. Therefore, these reactions produce the same rates for both models.

III. METHOD OF SOLUTION

The partial differential equations (pde's) described above are solved using a Method of Lines (MOL) approach. This solution scheme was chosen for several reasons. The method allows a great deal of flexibility in formulating the physics of a given problem. Many changes in physics are easily implemented. The method can naturally handle 1, 2 or even 3 space space dimensions as well as the various time scales present in the problems of interest. Finally, the method has been successfully applied to the related problem of oil shale retorting by Johnson and Hindmarsh (1983).

The Method of Lines solution scheme is based on the solution of a set of initial value ordinary differential equations (ode's). These ode's are obtained from the pde boundary value problem of interest by discretizing the pde's in the spatial dimensions. This yields a set of ode's with time as the independent variable. A suitable ode solver is then used to integrate the system of equations in time to yield the required results. The power of the method stems primarily from choosing one of the very powerful ode solvers currently available. The ode solver must be able to handle the stiff system which results from the discretization of the spatial dimensions and physics of the problem. It should also provide a straight forward method of time step and error control. The ode solver we have chosen, which meets these specifications, is LSODE a widely available software package developed at LLNL by Hindmarsh (1980). LSODE provides the user with a number of optional methods to be used in solving a system of ode's. We select option mf=25, which uses an internally generated banded Jacobian to solve a stiff equation set. The band width of our problem is related to the number of dependent variables selected as well as the number of cells in the x or radial direction.

The use of the Jacobian represents both the power and the limitation of the solution scheme. The Jacobian is a matrix defining the partial derivative of dependent variables with respect to other dependent variables and represents a method by which the equations to be solved are linearized, a key step in the solution of the ode's. However the size of the Jacobian can get quite large. For our problem the major computer storage limitation comes in dealing with

the storage of this Jacobian. The number of floating point values (fp's) required by LSODE for this and other purposes is given approximately for our problem by the formula

$$fp's = 10\ n_{eq} + 3\ (n_x+2)\ (n_v-1)\ n_{eq}$$

where n_{eq} is the number of equations, n_v is the number of dependent variables in the problem, and n_x is the number of cells in the x-direction. The number of equations, n_{eq} to be solved by LSODE is given by

$$n_{eq} = n_x \cdot n_y \cdot n_v$$

where n_y is the number of cells in the y-direction. For a one dimensional problem this size constraint is not serious. For a problem in which seven gas species are used a 360 cell problem can be contained entirely in the memory of a 400k word CDC 7600 and a 1800 cell problem in a 2 million word CRAY. Size constraints however are much more limiting for a two dimensional problems. For a 7 gas species problem only a 11x8 ($n_x n_y$) problem can fit on the CDC 7600 and a 41x11 problem on a CRAY. If, however, only three gas species are required in a two dimensional problem then a 11x21 problem will fit of the CDC 7600 and a 11x101 problem on the CRAY.

Unlike the computer memory requirements, general statements cannot be made on computation time requirements, because the computation time depends not only on the problem size but the problem physics. As an example, a 1 mol/s-m^2 flow of 2:1 steam:oxygen mixture would gasify 1/3 of a one-dimensional char bed 1 meter long in 8 hours. The computation times on CDC 7600 time for this gasification process using seven species were 363 s for 11 nodes, 1105 s for 21 nodes, and 2845 s for 41 nodes. These times are larger than previously reported in Thorsness and Kang (1984). Analysis reveals that only a small increase in computation time was due to variable properties; rather, the more stringent error control currently being applied in LSODE seems to be causing increased computation times. A further feel for computation time is provided in the following discussion of the validation and example runs.

In developing the discretized equations fairly standard finite difference methods were used. Wherever possible the conservative nature of the equations was preserved. Also upwind or donor cell differencing of the convective terms was used to protect against the formation of spatial wiggles in convected quantities. Spatial wiggles cannot be tolerated since they can lead to nontrivial negative concentrations which are difficult to handle. The price paid for removing the wiggles in this fashion is an increase in numerical dispersion, which can only be reduced by using finer cells. The details of the differencing used as well as boundary value treatment are given in Appendix C.

The computer code which was generated to perform the required calculations is quite flexible. A large variety of boundary conditions, initial conditions, geometry and problem physics can be specified through the input data. This includes the ability to select from a list of seven gas species built into the code. For problems requiring only a few gas species the ability to solve the equations for only a selected set of gases can lead to a large savings in computer resources. The code is modular enough that additional gas species and new kinetic or transport correlations can easily be added. This however does require a recompilation. The code is designed so that a given problem can be repeatedly restarted from any desired point in its evolution and new problem parametrs can be specified. This can greatly reduce the computational effort in doing parameter studies as well as provide a means to recover from minor computing problems that may arize. Finally, to maximize flexibility of output, two post-processor codes are used to tabulate or plot selected data from computed results. These codes can be run repeatedly to display different aspects of a single computational run.

As a result of the robust nature of the solution scheme, few compromises had to be made in the physical description of the problem to fascilitate the numerical solution. Two such features, however, have been added: (1) In the reaction rate routine special coding is present so that two small negative reactant concentrations do not result in a positive rate; (2) An artificial mass transfer resistance has been added to the gas phase oxidation rate

expressions. This is modeled after the gas-film resistance of the heterogeneous reactions and is a simple way of limiting the oxidation reaction rate at high temperatures. This resistance is controlled through an input parameter so that it offers no resistance, is equal to that for the heterogeneous reactions, or any fraction of the gas-film resistance of the heterogeneous reactions. This allows the gas-phase oxidation to be finite yet prescribed so that it is everwhere some multiple times larger than any of the heterogeneous rates. We usualy set the parameter to 0.2, limiting the gas-phase oxidation rates at least five times larger than any of the heterogeneous reactions. As a final practical matter we have found that on occasion the calculation will sometimes yield a branch solution with negative concentrations. Our code can detect this, and restarting the problem at a point just prior to the problem area provides a successful solution.

IV. VERIFICATION RUNS

In this section we present results of various runs made to ascertain the generality of the present formulation for many physical situations taking place in packed beds. These aspects involve not only steady and transient gas flows, but also reactions, moving waves (with widely diverse time constants), one and two (including axisymmetric) dimensions, and wall interactions. We also determine the effects of mesh sizes on the accuracy and CPU for the diverse physical situations. Applications of the present method to problems related to UCG are discussed in the following section.

Before giving specific details, we list cases analyzed to validate the models and numerical methods embodied in the GSF code. These are:

1. One-dimensional, Steady Flow;
2. One-dimensional, Transient Concentration Wave Motion;
3. One-dimensional, Transient Thermal Wave Motion;
4. One-dimensional, Steady Flow with Wall Heat Transfer;
5. One-dimensional, Catalyst Regeneration Problem;
6. Two-dimensional, Steady Heat Transfer Phenomena;
7. One-dimensional, Gasification Problem.

The basis for choosing these cases is to investigate Eqs.(1)- (6), separately and together, to ascertain the versatility of the present approach to accommodate widely varying flow and reacting conditions.

The reference physical conditions used for these validation runs are :

Viscosity	$\mu = 5.4\ (10^{-5})$ kg/m-s;
Permeability	$r = 1.0\ (10^{-11})$ m^2;
Exit pressure	$P_e = 1.0\ (10^5)$ Pa;
Temperature (initial)	$T = 300$ K;
Flow rate	$G = 1$ mol/m^2-s;
Tube length	$L = 1$ m;
Tube width (or radius)	1 m;
Original gas in tube	Nitrogen (inert);
Effective mass dispersion	$D = 5.0(10^{-4})$ m^2/s;
Effective thermal conductivity	$k = 5$ W/m-s;

Unless otherwise noted, these values were used for all cases.

(1). <u>One-dimensional Steady Flow</u>.

This simple case is considered here to verify the overall gas flow Eq.(1). The physical situation studied is ;

One-dimensional;
Steady state;
No reactions;
No solid motion;
Isothermal;
No new gas introduction into the flow from the wall boundary.

Under these conditions all equations but one become superfluous. Only Eq.(1) remains nontrivial. Thus, Eq.(1) reduces to :

$$0 = - d(CU)/dy \qquad (25)$$

Integrating once, we get

$$C\ U = \text{const} = G \qquad 26)$$

where both C and U are a function of distance y. In order to obtain the flow field description, we choose the pressure P as the depenedent variable. The pressure is related to the velocity U from Darcy's law, Eq.(7) :

$$U = -\frac{\Gamma}{\mu}\frac{dP}{dy} \qquad (27)$$

Combining the Eqs.(6),(26) and (27), we get

$$\frac{dP^2}{dy} = -\frac{2\mu RTG}{\Gamma} = \text{constant} = A \qquad (28)$$

with the boundary condition $P=P_e$=constant at y=L.

The solution to the differential equation is

$$P(y) = \sqrt{P_e^2 + A(L-y)} \qquad (29)$$

We now compare this analytic solution with the GSF code calculation results, as shown in Figure 7, in which the GSF code also calculates the transient behavior of the pressure buildup inside the bed before reaching the steady state. Although 51 nodes are used, only the results at certain selected points are shown in the figure for clarity. Very good agreement is noted between the calculated results and the analytical solution at steady flow.

(2). Motion of a Transient, One-dimensional Concentration Wave.

When a gas is injected into a packed bed filled with an inert gas different from the injected gas, diffusion as well as convection of the injected gas takes place as it flows through the packed bed. Such a situation is considered here, i.e.,

One dimensional;
No reactions;
No solid motion;
Isothermal;
Injected gas = oxygen;
Original gas in bed = nitrogen;
Axial dispersion;
Constant porosity.

Under these conditions the only nontrivial equation is the species equation (2), which reduces to :

$$\frac{\partial c_i}{\partial t} + v\frac{\partial c_i}{\partial y} = D\frac{\partial^2 c_i}{\partial y^2} \tag{30}$$

with the boundary conditions

$t = 0;\ c_i = c_0$

$y = 0;\qquad vc_i - D\partial c_i/\partial y = vc_{in}$

$y = L;\qquad \partial c_i/\partial y = 0$

Equation(30) has been solved analytically by Brenner (1962) for these boundary conditions, i.e.,

$$\frac{c_i(y.t) - c_{inj}}{c_o - c_{inj}} = 2e^{B(2Y-\Theta)}\sum_{k=1}^{\infty}\frac{Ba_k[a_k\cos(2a_kY) + B\sin(2a_kY)e^{-a_k^2\Theta/B}]}{(a_k^2 + B)(a_k^2 + B^2 + B)} \tag{31}$$

where $Y=y/L$, $\theta=tv/L$, $B=vL/(4D)$, and the eigenvalue a_k can be determined from the transcendental relation

$$\tan(2a_k) = \frac{2a_kB}{(a_k^2 - B^2)} \tag{32}$$

The solution given in Eq.(32) converges slowly. For large B and/or small θ, it can be approximated by

$$\frac{c_i(y,t) - c_{inj}}{c_o - c_{inj}} = 1 - \frac{1}{2}\text{erfc}[(Y-\theta)\sqrt{\frac{B}{\theta}}] - \sqrt{\frac{4B\theta}{\pi}}\exp[-(Y-\theta)^2\frac{B}{\theta}] + \frac{1}{2}[1 + 4B(Y+\theta)]\, e^{4B\theta}\text{erfc}[(Y+\theta)\sqrt{\frac{B}{\theta}}] - 2\sqrt{\frac{4B\theta}{\pi}}[1 + B(2-Y+\theta)]\exp[4B - \frac{B}{\theta}(2-Y+\theta)^2] + 2B[2(2-Y+\theta) + \theta + 2B(2-Y+\theta)^2]e^{4B}\text{erfc}[(2-Y+\theta)\sqrt{\frac{B}{\theta}}] \qquad (33)$$

We shall use the latter asymptotic solution for comparison with the GSF code calculation results. The specific conditions used are: C = 12 mol/m^3, D = 5.0(10^{-4}) m^2/s, v = 0.8 m/s. Figure 8 shows the analytic solution as well as the GSF results with 26 and 201 nodes at t = 15 seconds. For the latter case only selected points are plotted in the figure for clearer comparison. The case of 25 nodes is reasonably close to the analytical solution, but much better agreement is noted between the analytical solution and the 201-node case. The CPU times on a CDC-7600 for these waves to encompass the entire bed (L=1 m) were 14 s for 26 nodes, 28 s for 51 nodes, 63 s for 101 nodes, and 176 s for 201 nodes. This indicates that increasing the number of nodes increases the CPU by a factor slightly greater than the node multiplication factor.

(3). Transient, One-dimensional Heat Wave .

This case considers a timewise motion of a heat wave travelling down a packed bed when a "heat load" (i.e., increased temperature) is imposed at the inlet location. We expect a wave motion similar to the above-analyzed motion of a concentration wave, but with a different wave velocity due to different physical factors affecting the heat transport processes. Again the heat wave is allowed to "disperse" in the axial direction (effective thermal conduction) as it flows downstream with a given gas flux value. In particular, we analyze the case of:

One dimensional;
No reactions;
No solid motion;
No new gas introduction;
No gas diffusion;
Gas in bed = nitrogen;
Constant axial thermal dispersion;
Constant physical properties.

Under these conditions the only nontrivial equation, Eq.(5), reduces to :

$$[\phi\rho_g c_g + (1-\phi)\rho_s c_s]\frac{\partial T}{\partial t} + \rho_g c_g U\frac{\partial T}{\partial y} = k\frac{\partial^2 T}{\partial y^2} \tag{34}$$

with the boundary conditions

$$t = 0;\ T = T_0;$$

$$y = 0:\ UC_g T - k\frac{\partial T}{\partial y} = UC_g T_{inj}$$

$$y = L:\ \frac{\partial T}{\partial y} = 0.$$

Equation (34) can be recast into a form amenable to solution, i.e.,

$$\frac{\partial T}{\partial \Theta} + U\frac{\partial T}{\partial Y} = k\frac{\partial^2 T}{\partial Y^2} \tag{35}$$

where the term θ is defined to be

$$\Theta = t\left[\frac{\rho_g c_g}{\phi\rho_g c_g + (1-\phi)\rho_s c_s}\right]$$

The analytic solution to Eq.(35) is, again from Brenner (1962):

$$\begin{aligned}\frac{T(y,t) - T_{inj}}{T_o - T_{inj}} = 1 &- \frac{1}{2}\operatorname{erfc}[(Y-\Theta)\sqrt{\frac{B}{\Theta}}] \\ &- \sqrt{\frac{4B\Theta}{\pi}}\exp[-(Y-\Theta)^2\frac{B}{\Theta}] \\ &+ \frac{1}{2}[1 + 4B(Y+\Theta)]\, e^{4B\Theta}\operatorname{erfc}[(Y+\Theta)\sqrt{\frac{B}{\Theta}}] \\ &- 2\sqrt{\frac{4B\Theta}{\pi}}[1 + B(2-Y+\Theta)]\exp[4B - \frac{B}{\Theta}(2-Y+\Theta)^2 \\ &+ 2B[2(2-Y+\Theta) + \Theta + 2B(2-Y+\Theta)^2]e^{4B}\operatorname{erfc}[(2-Y+\Theta)\sqrt{\frac{B}{\Theta}}]\end{aligned} \tag{36}$$

where Y=y/L and B=UL/(4D), as previously defined before. Figure 9 shows the analytical solution and the GSF results at t = 4500 s, for 26 nodes and 201 nodes in a packed bed. The original bed and gas temperature is at 300 K, and the injected temperature at the inlet is 600 K. Very good agreement is seen between the analytical results and the code calculations, especially the 201-node case.

Note the similarity of the shapes between the thermal waves and the concentration waves. Physically, however, there is a great difference between these two wave motions, i.e., the time scale of motion. Whereas the oxygen wave moves through the bed in less than a minute, the thermal wave moves much more slowly, consuming more than two hours to encompass the length of the bed (L=1 m). This is due to the large heat capacity of the solid particles consituting the packed bed. The CPU times for the GSF runs on 7600 computer were 19 s for 26 nodes, 42 s for 51 nodes, 107 s for 101 nodes, and 202 s for 201 nodes.

We thus conclude that the GSF code can calculate and produce similar solutions (e.g., the thermal and concentration waves), by integrating different PDE's with widely variant propagation velocities.

(4). <u>One-dimensional Flow with Wall Heat Transfer</u>.

This is a quasi-two dimensional situation in that although the flow is one dimensional, the thermal-energy exchange with the wall is accounted for by use of a heat-transfer coefficient and the local temperature difference between the flow and the wall temperatures. The specific conditions studied are :

Steady state;
Constant wall temperature;
One-dimensional;
No reactions;
No solid motion;
No new gas introduction;
One gas species (nitrogen);
No species diffusion;
Constant physical properties.

Under these conditions only Eq.(5) is non-trivial, and we have:

$$k\, d^2T/dy^2 - (CUc_g)dT/dy - (hA_s/A_c)(T - T_w) = 0 \qquad (37)$$

where the term h denotes the heat-transfer coefficient (taken to be a constant here), A_s/A_c the ratio of the bed surface area to the cross-sectional area of the bed, and the other terms have their usual meanings.

Two different boundary conditions are treated at the exit plane: (1) zero temperature gradient ; and (2) radiative heat exchange with the surroundings. We will see that not only different solutions are obtained, but also quite different temperature distributions prevail inside the bed, depending on the boundary conditions.

(Case 1). Zero temperature gradient at exit.

$$\text{inlet } (y = 0) \; ; \quad C\, c_g\, U\, T_{inj} = C\, c_g\, U\, T - k\, dT/dy$$

$$\text{exit } (y = L) \; ; \quad dT/dy = 0$$

The analytic solution to Eq.(37) with the above boundary conditions is :

$$T(y) - T_w = (T_{inj} - T_w)\{A \exp(-E_3 y/2) - B \exp(E_2 y/2)\} \qquad (38)$$

where $p = C\, c_g\, U/k$; $q = (h\, A_p/k\, A_c)$;

$E_1 = (p^2 + 4q)^{1/2}$; $E_2 = E_1 + p$; $E_3 = E_1 - p$;

$E_4 = 1 + E_3/(2p) - (1 - E_2/(2p))(E_3/E_2) \exp(-E_1 L)$;

$A = 1/E_4$; and $B = E_3 \exp(-E_1 L) / (E_2\, E_4)$.

Figure 10 shows the GSF results and the analytical solution for the case of the inlet temperature at 1000 K and the wall temperature at 900 K. Good agreement is seen from the figure.

(Case 2). Radiative Loss at Exit.

$$\text{inlet } (y = 0) \; ; \quad C\, c_g\, U\, T_{inj} = C\, c_g\, U\, T - k\, dT/dy;$$

$$\text{exit } (y = L) \; ; \quad -k\, dT/dy = S\,(T^4 - T^4_{ambient}).$$

where the term S is a function denoting combination of the radiation shape factor, the emissivity of the flowing gas, and the Stefan-Boltzmann constant, see Eq.(21).

The analytic solution to Eq.(37) with this radiative boundary condition can be obtained from solution of quartic expressions for the temperature term, and is given in Appendix E.

Figure 10 also shows the analytic solution for exit conditions of 0.7 emissivity and unity view factor. In contrast to the previous case of no radiation loss at the exit plane, in which the temperature distribution inside the bed was always above the wall temperature, the radiative case shows that the bed temperature can become lower than the wall temperature due to large radiative heat loss at the exit plane to the ambiemnt surroundings. In fact the present particular example shows that the exit temperature goes down to 738 K, much lower than the 900 K wall temperature. Figure 10 also shows the GSF code results for 51 nodes in the bed. Good agreement is again noted.

(5). Catalyst Regeneration Problem .

This problem is often encountered in designing reactors for cracking or dehydrogenating hydrocarbons, where regeneration is employed to remove coke deposits form the catalyst bed. Removal is effected by oxidation, which generates a high temperature peak in the reaction zone where burning of the coke is taking place. This reaction zone then travels down the bed, purging coke in its path. Such a case is studied here, i.e., the regeneration of a

catalyst bed by oxidation of contaminants. The problem is idealized to the case of introducing oxygen and nitrogen at the inlet of a packed bed containing inert particles with a small fraction of carbon. The bed is initially at temperature T_0. Only carbon combustion is allowed, i.e., $C+O_2 \rightarrow CO_2$ reaction.

For analytic case the specific conditions used are:

One dimensional;
Constant flow rate;
Constant properties;
No solid motion;
No mass dispersion;
No thermal dispersion;
Two gas species (oxygen and nitrogen);
Carbon combustion only;
Zero-order reaction (independent of temperature).

Under these conditions Eq.(2) becomes :

$$\frac{\partial(\phi c_{o^2})}{\partial t} = -\frac{\partial(Uc_{o^2})}{\partial y} + s_{o^2} \tag{39}$$

Eq.(4) becomes:

$$\frac{\partial[1-\phi_o)\rho_s w]}{\partial t} = s^* \tag{40}$$

Eq.(5) becomes:

$$[\phi\rho_g c_g + (1-\phi_o)\rho_s c_s]\frac{\partial T}{\partial t} = -\frac{\partial(U\rho_g c_g T)}{\partial y} + \rho_s L^* B \tag{41}$$

where L^* denotes the heat of reaction and B the production (or loss) rate of carbon. The term B will be defined subsequently. Since oxygen and solid carbon react with each other in combustion, s_{o2} and s^* are related to each other and to B.

Rearranging and introducing new symbols (for this problem only), we obtain:

$$\phi\rho_g\frac{\partial z}{\partial t} + G\frac{\partial z}{\partial y} = -B\frac{M_g}{M_c}\rho_s \tag{42}$$

$$\frac{\partial H}{\partial t} = -B \tag{43}$$

$$\rho_s c_s\frac{\partial T}{\partial t} + c_g G\frac{\partial T}{\partial y} = \rho_s L^* B \tag{44}$$

where Z is the mole fraction of oxygen, H the carbon content (kg/kg-catalyst), and $B=kPZH/H_0$, H_0 being the initial carbon content in the bed.

The boundary conditions for this traveling reaction wave are:

$t = 0$: $Z = 0$ and $T = T_0$;

$t - Z/v \leqslant 0$: $H = H_0$;

$y = 0$: $Z = Z_0$ (Oxygen injection at inlet).

The term v denotes the gas velocity in bed, i.e., $v = G/(\rho_g\phi)$.

Introducing new variables, the differential equations (42)-(44) become:

$$\partial Z/\partial\xi = -\lambda Z \tag{45}$$

$$\partial\lambda/\partial\tau = -\lambda Z / Z_0 \tag{46}$$

$$M\,\partial\Omega/\partial\tau + S\,\partial\Omega/\partial\xi = \lambda Z / Z_0 \tag{47}$$

where

$\lambda = H/H_0$,

$\Omega = (T-T_0)\ c_s/(L^*\ H_0)$,

$\xi = y\ (\rho_s\ M_g\ k\ P/G\ M_c)$

$\tau = (Z_0/H_0)\ k\ P\ (t - y\ \phi\rho_g/G)$

$M = 1 - (c_g\phi\rho_g/c_s\rho_s)$

$S = (M_g\ c_g\ H_0/M_c\ c_s\ Z_0)$

The solutions to these equations are, from Johnson et al (1961):

$$Z_0/Z = 1 + e^{-\tau}(e^{\xi}-1) \tag{48}$$

$$H_0/H = 1 + e^{-\xi}(e^{\tau}-1) \tag{49}$$

The temperature solution is generally more complicated; however, for the special case of M=1, S=1, and all combustion proceeding to CO_2, a closed-form solution to Eq.(47) can be obtained from Thorsness, et al (1978);

For $\tau \leq \xi$:

$$\frac{T-T_0}{L^*H_0/c_s} = \frac{e^{\xi-\tau}}{(1+e^{\xi-\tau})^2}\left[\ln W - \frac{1}{W}\right]_{W=e^{\xi-\tau}}^{W=e^{\tau}+e^{\xi}-1} \tag{50}$$

and for $\tau > \xi$:

$$\frac{T-T_0}{L^1 H_0/c_s} = \frac{e^{\tau-\xi}}{(1+e^{\tau-\xi})^2} \left[\ln W - \frac{1}{W} \right]_{W=e^{\xi}}^{W=e^{\tau}+e^{\xi}-1} \qquad (51)$$

Using the GSF code, sample calculations were performed for initial bed temperature of 600 K, giving a reaction wave which proceeds downstream as a function of time. Results are given in Figures 11 and 12 at t = 427 sec with 101 nodes for the GSF code calculations. Figure 11 shows the carbon and the oxygen distributions along the bed. Also shown is the analytic solution, which compare favorably with the GSF results. The temperature distribution is given in Figure 12. The profiles agree well with each other except in the reaction region, where the analytic result is more peaked than the GSF result. This discrepancy can be attributed mainly to the fact that the upwind difference used for stability in GSF code unavoidably introduces some dispersion into the problem. This dispersion can only be made identically zero by using an infinite number of nodes. In real systems some dispersion is always present; however, the analytic solution is only exact for zero dispersion. Therefore, the agreement is deemed acceptable.

(6). Steady, Two-dimensional Flow with Wall Heat Transfer.

This type of flow is often employed to measure the effective thermal conductivities in packed-bed flow situations (e.g., Wakao and Kaguei 1982). Consider a cylindrical packed bed operated as a steady-state heat exchanger, that is,

Steady state;
Uniform flow;
No reactions;
No new gas introduced;
No solid motion;
Constant wall temperature;
One gas species (nitrogen);
Constant physical properties.

Under these conditions only Eq.(5) is nontrivial, it reduces to:

$$G c_g \frac{\partial T}{\partial y} = \frac{1}{x}\frac{\partial(x k_x \partial T/\partial x)}{\partial x} + k_y \frac{\partial^2 T}{\partial y^2} \qquad (52)$$

with the boundary conditions

$x = 0$ (centerline): $\partial T/\partial x = 0$ (symmetry condition);

$x = R$ (wall): $- k_x \partial T/\partial x = h\ (T - T_w)$;

$y = 0$ (inlet): $T = T_0$.

The last condition states that the inlet temperature is maintained at a prescribed value T_0. (Usually the inlet temperature is different from the injected temperature by the thermal gradient exisitng at the inlet.)

Analytic solution to Eq.(52) with these boundary conditions is given in Wakao and Kaguei (1982):

$$\frac{T - T_w}{T_0 - T_w} = 2 \sum_{n=1}^{\infty} \frac{J_0(a_n x/R) \exp(-a_n^2 Z)}{a_n J_1(a_n)\,[1 + (a_n/B)^2]} \qquad (53)$$

where $B = h\ R\ k_x$; and

$$Z = \frac{2\ y\ k_x / (G c_g R^2)}{1 + [1 + 4\,(\frac{a_n}{G c_g R})^2\ k_x k_y\ ]^{1/2}}$$

and the roots of the coefficients in the Bessel solution can be obtained from the transcendental relation

$$B\ J_0(a_n) = a_n\ J_1(a_n).$$

For large y, i.e., some distance from inlet, the analytic solution can be simplified to:

$$\frac{T - T_w}{T_0 - T_w} = \frac{2\ J_0(a_1 x/R) \exp(-a_1^2 y)}{B\ J_0(a_1)\,[1 + (a_1/B)^2]} \qquad (54)$$

It will be seen that this simpler solution is adequate for most of the length of the packed bed.

Sample calculations were made on GSF code for a bed (0.5 m long) initially at 900 K. At time t = 0, the inlet temperature is raised to, and maintained at, 1000 K. The results are shown in Figure 13, which shows a slow decrease in the centerline temperature along the bed, while the near-wall temperature shows a steep decrease immediately after the inlet region, reflecting strong heat-transfer activity there. When we compare the results from the GSF code (with 6 x 21 nodes) with the analytic solutions, we obtain good agreement everywhere except near the inlet region. This discrepancy is due to the use of a simpler analytic solution, which assumes identical injected gas and bed-bottom temperatures. Despite this, the two results are close enough to confirm that the present GSF code can calculate accurately the two-dimensional heat transfer situations in a packed bed.

(7). Steady, One-dimensional Gasification Problem.

A number of quasi-steady one dimensional gasification models have been developed over the past few years. The models are quasi-steady in that they assume that in a coordinate system translating at the proper velocity the gasification waves will appear to be unchanged with time. Recently Britten (1985) has developed such a model based on physical submodels essentially the same as those used in GSF. Although the physics is basically the same the method of solution is entirely different, in that the equations reduce to ode's and a shooting method relying on repeated integration of the equations in the space dimension is used. Comparison of the GSF results with results of this alternate solution should prove useful in validating both solution schemes.

The basic assumptions made for this case are:

One dimensional;
Constant injection rate;
No mass dispersion;
Three gas species (O_2, CO and CO_2);
Constant properties;

In the simplified model of Britten, CO plays the role of both (CO and H_2, while CO_2 plays the role of CO_2 and H_2O, the intent being to compute the total conversion to CO and H_2 not their specific ratios. Britten also uses a composite gasification rate for char gasification given by the steam gasification kinetics. Input values for this run were 25% oxygen and 75% steam at 1 mol/m^2-sec.

The GSF results were computed using five gas species N_2, O_2, CO, H_2, and CO_2The N_2 and H_2 were everywhere zero. The GSF results reach an essentially quasi-steady nature after approximately 2.5 hours of gasification starting from a bed initially at 1000 K. In Figure 14 the results of the two models are compared in terms of dimensionless values for temperature, gas composition, and carbonfraction. The results of the Britten model have been shifted arbitrarily on the position axis since they are taken as completely quasi-steady. The agreement, especially near the gasification front, is excellent. There is some discrepancy on the downstream end. This is attributed to a slightly different treatment of the details of the gasification kinetics and the unavoidable difference in treatment of the downstream boundary conditions.

For the GSF results 39 cells were used and because of the high degree of accuracy desired at peak 20 minutes of CDC 7600 time were required.

V. SAMPLE PROBLEMS RELATED TO UCG

Now that we have made some attempts to validate parts of the GSF model and numerical approach, we apply the code to several disparate situations which have bearing on the underground coal gasification processes. These cases are: wall drying, wall regression during gasification, and water injection into a gasifying bed. In what follows, we treat these cases in detail.

(A). Transient Water Injection during Gasification.

One of the factors affecting the underground coal gasification processes is the water influx into the active gasification zone. The transient response of the reacting flow inside a packed bed is calculated here as an application of

the present approach to the water injection problem. Some experiments and theoretical calculations have been made by Edgar, et al.(1985). We consider the following situation:

One dimensional;
No pyrolysis.

The gases are composed of 7 species, undergoing 8 reactions, in a packed bed of 0.15 m long with 0.05 m diameter. The initial temperature is 900 K.The flow begins at t = 0 with the inlet gas (26 % oxygen, 74 % water vapor) being injected at a steady rate of 1.5 (10^{-3}) mol/s. The char then reacts with the incoming gases to produce CO, CO_2, H_2, and CH_4 in the bed. The gasification front moves down the bed, consuming carbon in the process. At t = 3500 sec, when the product gases (at the exit) have reached a reasonably steady state, we inject water at the midpoint of the bed, slightly downstream of the reaction front. We assume that the liquid water influx is instantly turned into water vapor, and it is this injected steam (taken to be 8(10^{-4}) mol/s in this example) that reacts with the char and the gases flowing from upstream.

Calculations were performed on the GSF code with 11 nodes. Results are shown in Figure 15, where the various gas species are plotted as a function of time. The sudden changes in CO and the more gradual change in the H_2 gases are noted. While the water vapor injection (at the midpoint of the bed) is continuing, the CO and CO_2 mole fractions are seen to approach steady values, whereas that for the H_2 gas is still decreasing. When the midpoint injection is turned off at t = 5500 sec, the gases undergo changes which eventually return them to pre-injection conditions. However, in this particular example, the reaction front has reached the exit region at about t = 7200 sec, so that the gas flowing out of the exit is composed of 26 % oxygen and 74 % water vapor,i.e., the inlet gases. The carbon consumption history is plotted in Figure 16, and shows a steady decline in the amount of char available for gasification. These results, while appearing to be physically reasonable, are not intended as the definitive description of what takes place in the bed when water is injected. We defer extensive physical

interpretation to a later date. Rather, they are presented here to demonstrate the calculational capabilities of the GSF code, for the case of water injection into the bed during active gasification.

(B). Wall Drying.

Understanding the physics of cavity growth at the wall of a rubble filled gasification cavity is of importance in determining ultimate cavity width and thus resource recovery in in-situ coal gasification. Grens and Thorsness (1984) have suggested that the growth is directly linked to the rate of heat transfer from a hot rubble bed to a drying/pyrolyzing coal wall. To explore the fundamentals of this mechanism a series of experiments is being undertaken at the University of California, Berkeley under Prof. Grens. The first in this series of experiments will look at the simple model system of a uniform non-reacting bed with hot gas folowing through it and a water saturated wall. The rate of drying of the wall and thus the rate of heat transfer to the wall will be examined in a cylindrical vessel with the hot gas flow entering at the bottom center.

GSF has been used to do some preliminary modeling of a related system. We assumed a cylindrical reactor of radius 5 cm and height 25 cm filled with a low density spherical packing 1.25 cm in diameter creating a uniformly permeable bed. The walls are assumed to be kept saturated with water and are evaporating into the hot gas flow. 8 mmol/s (1 mol/s-m^2 of bed) of gas are assumed injected at 900 K while the initial bed temperature is 300 K. The wall model described in Appendix D is used to apply boundary conditions at the evaporating walls. The bottom of the bed is assumed to operate adiabatically. The injected gas is assumed to be nitrogen. Preliminary runs indicated that results obtained assuming only one gas species gave essentially the same results as that for the two gases, N_2 and H_2O, system so, to save computer resources runs were made using a one gas system.

Many runs were made using a variety of cell numbers. All of these runs eventually reached a steady-state solution. The results show that the average drying rate can be fairly well estimated even with a very coarse 3x3 system.

In Figures 17-20, selected results computed using a 6x11 system are presented. In Figure 17 the time to reach steady-state is compared for a range of injected gas flow rates. As one would expect the time to reach steady-state increased rapidly with decreasing flow rate, ranging from about 100 seconds for the 10 mol/s-m^2 case to 5,000 seconds (2.8 hrs) for the 0.1 mol/s-m^2 case.

Figure 18 shows the average wall drying rate as a function of injected gas flow. The slope of the flow rate versus drying rate on the log/log plot ranges from about 1 at the low flow to about 0.8 at the high flow. The 0.8 power dependence at the high end is clearly consistent with the heat transfer correlation 0.8 dependence described in Appendix D. On the low flow end the unity power dependence is not a result of the heat transfer flow dependence which is 0.5, but rather reflects the fact that the limiting factor is total heat injected. That is, at the very low flows the exit gas leaves the bed at the steam temperature and thus the drying rate is limited by the available energy in the injected hot gas.

In Figure 19 the local evaporation rate versus vertical position in the bed is shown at steady state for three flow rates. As would be expected the rate is more uniform at the high flow where the energy input is not limiting. In Figure 20 the calculated wall and center-line temperatures are plotted for the three flow rates. The heat limitation is clearly shown here by the coincidence of the wall and center line temperatures near the top of the bed for the low flow case.

(C). Wall Regression during Gasification.

The final example demonstrates GSF's ability to perform calculations for an axi-symmetric gasifying bed. The problem of interest here is related to small cavities and to our proposed simulated coal seam experiments. These experiments would utilized a synthetic coal seam approximately 5 ft (1.5 m) thick. The model system on which calculations were performed is 1 meter in radius and 1 m high. It is filled with rubble material consisting of ash in the center and char near the walls and at the top. The walls are coal which can pyrolyze and produce gas and char. A 2:1 steam:oxygen mixture is injected at a rate of 6 mol/s into the bottom center of the bed. A series of runs were performed to determine what thickness of char bed at the wall would lead to a

self sustaining system. What is meant here by self sustaining is simply that calculated char bed production at the wall, estimated via the wall model of Appendix D, is equal to the rate of char bed consumption near the wall but in the bed.

Calculations were performed using all seven gas species on a coarse 6 x 6 grid. The initial bed temperature was set at 900 K so that the bed would reach a fairly steady thermal profile before too much of the bed carbon was consumed. A fairly steady-state was reached after about one hour of real time. To compute the complete transient during start-up leading to this steady-state required 35-40 minutes of computer time on a CDC 7600 machine.Figure 21 shows the rate of carbon production computed at the walls and the amount of carbon consumed in the bed as a function of three assumed char layer thicknesses. The computed wall regression rate, and thus the computed carbon production rate, was very nearly constant in all three cases, while the carbon consumption varied more or less linearly with char thickness. The linear variation of carbon consumption is clearly related to the greater abundance of carbon in the bed and the decrease in distance between the injection point and the char/ash transition. The wall regression rate indicates that the dominate resistance for heat transport to the coal wall is the wall layer heat transport and not the proximity of the char/ash transition. The figure indicates that the run made with a wall char bed thickness of 7.5 cm is close to a self sustaining system, at least on the average, since the rate of carbon consumption is very nearly equal to the carbon production.

The bed temperature isotherms and gas fluxes near steady-state are shown in Figures 22 and 23, respectively, for the 7.5 cm char thickness run. The gas injection temperature is 400 K and the computed average wall temperature is 1100 K while the exit gas temperature is 1700 K. The temperature gradient near the wall is not well represented by the coarse isotherms of Figure 22. The sharp gradient at the bed top is a result of the char layer present at the bed top. Although the average carbon consumption and production are nearly balanced for the 7.5 cm case, local rates show some variation. In particular the amount of carbon loss from the bed exceeds the local carbon production at

the wall in the bottom portion of the bed. This local disparity is shown in Figure 24. The rates over the top portion of the bed are, however, very nearly equal. This behavior indicates that the char layer would tend to be thinner near the bed bottom.

Also shown in Figure 24 is the computed local wall regression rates. They indicate that the bed wall would move outward more rapidly at the top than at the bottom in a truly self sustaining system. Also note that the average wall regression rate of 7.7×10^{-7} m/s is only 0.07 m/day. This is a very low rate and suggests that in order to obtain higher rates more characteristic of field results ($\sim$ 0.5 m/day) some additional physics not currently present in GSF must be involved. It is our feeling that the most likely candidate is a non-uniform permeability distribution. This hypothesis is explored in recent related modeling work to be found in Grens and Thorsness (1985).

VI. CLOSURE

We have presented details of generalized model formulation for describing reacting flows through packed beds. The model contains, among other things, physically reasonable wall transport, transient models, many reactions and species (including methane), various options on the boundary conditions, rezoning capability, and variable transport properties, including effective thermal and mass dispersions.

Results obtained from the present model (and the GSF computer code developed from the model) show wide applicability of the code for characterizing various reacting flows through packed beds. The situations we have tested are : concentration and thermal waves travelling at very different velocities, transient reacting wave motions, wall heat transfer, and wall regression processes. In all of these cases, the general model demonstrated its validity by comparing favorably with other available studies. The present code also demonstrated its workability for these disparate situations from the CPU standpoint with reasonable number of cell sizes describing a packed bed configuration.

The model has also been applied to the introduction of a fluid into the mid-point of a packed bed, and to the case of wall regression due to reactions at the wall surface. Some preliminary results are obtained which show promise; however, more analysis is needed before a definitvie statement can be made on the applicability of the present model to these cases. Future plans include : use of the GSF code for detailed examination of the phenomena taking place inside a synthetic coal (scale model); scoping of important machanisms for packed-bed flows at various conditions of temperature, pressure, particle size, etc., evaluating the validity of other simplified models. We also plan to investigate the feasibility of modifying the present upwind differencing capability to improve the numerical integration scheme, along with an alternative numerical approach which is more efficient from the computer storage and time management viewpoint. Other plans are to continue analysis of the peak-temperature near the reaction front, two dimensional drying problem, the wall-growth problem, incorporation of the momentum equation into the model rather than using the Darcy equation, and finally the water-influx problem involved in the underground coal gasification phenomena.

NOMENCLATURE

A	=	Pre-exponential rate constant	(1/s)
B	=	Reaction rate used in regeneration problem	(1/s)
C	=	Total gas concentration	(mol/m_3)
c_i	=	Concentration of gas species i	(mol/m_3)
c_{eq}	=	Equilibrium concentration of a gas	(mol/m_3)
c_g	=	Average gas heat capacity	(J/mol-K)
c_m	=	Effective heat capacity of material passing through the wall -- see Eq.(D.3)	(J/mol-K)
c_s	=	Average solid heat capacity	(J/kg-K)
D	=	Effective superficial mass dispersion in bed	(m^2/s)
D_e	=	Effective gas diffusivity inside a particle	(m^2/s)
D_m	=	Average molecular diffusivity	(m^2/s)
d	=	Diameter	(m)
d_a	=	Ash particle diameter	(m)
d_p	=	Particle diameter	(m)
d_u	=	Unreacted particle diameter	(m)
d_0	=	Initial particle diameter	(m)
E	=	Activation energy for rate constant	(J/mol)
F	=	Fraction of original carbon remaining	
f	=	Ash particle size fraction	
f_w	=	Mass fraction of water in the coal	
G	=	Average molar gas flux	(mol/m^2-s)
H_v	=	Heat of vaporization of water in the coal	(J/kg)
h	=	Heat transfer coefficient	(W/m^2-K)
h^o	=	Heat transfer coefficient corrected for high mass flux -- see Eq.(D.3)	(W/m^2-K)
h_i	=	Enthalpy of gas species i	(J/mol)
h_k^*	=	Enthalpy of solid species k	(J/kg)
j_i	=	Total flux of gas species i	(mol/m^2-s)
k	=	Effective bed thermal conductivity	(W/m-K)
k_c	=	Gas film mass transfer coefficient	(m^2/s)
k_r	=	Reaction rate constant	(1/s)

L^*	=	Heat of reaction	(J/kg)
M_i	=	Molecular weight of species i	(Kg/mol_i)
m	=	Number of solid species	
N	=	Number of particles per volume of bed	($1/m^3$)
N_a	=	Number of ash particles per volume of bed	($1/m^3$)
n	=	Number of gas species	
n_v	=	Numbeer od dependent variables	
n_x	=	Number of nodes in x-direction	
n_y	=	Number of nodes in y-direction	
P	=	Pressure	(Pa)
Q_d	=	Heat flux at drying front -- Eq.(D.1)	(W/m^2)
Q_f	=	Heat flux at wall -- Eq.(D.1)	(W/m^2)
Q_i	=	Rate of species introduced into flow	(mol/m^3-s)
R	=	Gas constant	(J/mol-K) or ($Pa-m^3/mol-K$)
r	=	Reaction rate per volume of bed	(mol/m^3-s)
r^*	=	Intrinsic reaction rate	(mol/m^3-s)
r_1^*	=	Intrinsic rate of reaction 1	(mol/m^3-s)
S	=	Dimensionless heat of vaporization -- see Eq.(D.9)	
Sc	=	Schmidt number	
s_i	=	Species i gas source per volume of bed	(mol/m^3-s)
s_k^*	=	Solid species k source per volume of bed	(kg/m^3-s)
s_c^*	=	Solid carbon source per volume of bed	(kg/m^3-s)
T(x,y,t)	=	Temperature at position x,y at time t	(K)
T_b	=	Bulk-gas temperature in bed -- Appendix D	(K)
T_d	=	Drying-front temperature -- Appendix D	(K)
T_f	=	Wall failure temperature -- Appendix D	(K)
T_{inj}	=	Injected gas temperature	(K)
T_{sinj}	=	Temperature of input solid	(K)
t	=	Time	(s)
U	=	Superficial gas velocity	(m/s)
u	=	Wall recession rate -- see Appendix D	(m/s)
V	=	Gas superficial mass velocity in bed	(kg/m^2-s)
v	=	Effective gas velocity	(m/s)

v_{int} = Interstitial velocity (m/s)
v_s = Superficial solid velocity (m/s)
v_{s0} = Superficial solid velocity at the bottom of the bed (m/s)
W = Heat source introduced into the flow (W/m^3)
w_{a0} = Initial weight fraction of ash in solid
w_c = Mass fraction carbon in solid
w_{c0} = Initial weight fraction of carbon in solid
w_k = Mass fraction of solid species k
x = Horizontal coordinate (m)
y = Vertical coordinate (m)
y_i = Mole fraction of species i
α = Fraction of combusted carbon going directly to carbon monoxide
Γ = Permeability (m^2)
η = Reaction effectiveness factor
μ = Average gas viscosity (Pa-s)
ξ = Dried/pyrolyzed coal-layer thickness -- see Appendix D (m)
ρ = Gas density (kg/m^3)
ρ_s = Average density of solid particle (kg/m^3)
ρ_c = Carbon density in unreacted solid (kg/m^3)
ρ^* = Reactive solid density (kg/m^3)
τ = Thiele modulus
ϕ = Total porosity in the bed
ϕ_e = Bed porosity external to particles
ϕ_{int} = Porosity internal to a particle
ψ = Dimensionless temperature in coal layer -- Eq.(D.9)
Ω = Ratio of the heat carried by the mass flux into the bed to the gross heat flux to the wall by convective mechanism -- Eq.(D.3)

Subscripts

a = ash

c = carbon

e = external condition

g = gas

i = gas species: 1 - N_2;
2 - O_2;
3 - H_2;
4 - CO;
5 - CO_2;
6 - H_2O;
7 - CH_4

k = solid species: 1 - carbon;
2 - ash

s = solid

w = water

0 = initial condition

REFERENCES

Bischoff, K.B., and Levenspiel, O. (1962), " Fluid Dispersion - Generalization and Comparison of Mathematical Models - I ", Chem. Eng. Sci., 17, 245-255.

Bischoff, K.B.B.(1969), " A Note on Gas Dispersion in Packed Beds", Chem. Eng. Sci. J., 24, 607.

Brenner, H. (1962), " The Diffusion Model of Longitudinal Mixing in Beds of Finite Length. Numerical Values ", Chem. Eng. Sci. J., 17, 229.

Britten, J. (1984), "Modelling One-diemnsional Coal Gasification Process: No Gas-phase Dispersion Case ", LLNL UCG Monthly Report, Nov. 1984.

Calderbank, P., and Pogorsky, L. (1957), " Heat Transfer in Packed Beds", Trans. Inst. Chem. Engrs., 35, 195-205.

Colburn, A., and Drew, T. (1937), " The Condensation of Mixed Vapors ", Trans. AIChE 33, 197-212.

Coberly, C.A., and Marshall, W.R. (1951), " Temperature Gradients in Gas Streams Flowing through Fixed Granular Beds", Chem. Eng. Prog., 47, 141-150.

Deissler, R.G., and Boegli, J.S. (1958), " an Investigation of Effective Thermal Conductivities of Powders in Various Gases", ASME Trans., 1417-1425.

Denn, M., Wei, J., Yu W.-C., and Cwiklinski, R. (1982), " Detailed Simulation of a Moving-Bed Gasifier", EPRI Report AP-2576.

Dixon, A.G., and Cresswell, D.L. (1979), " Theoretical Prediction of Effective Heat Transfer Parameters in Packed Beds", AIChE J., 25, 663-676.

Edwards, M.F., and Richardson, J.F. (1968), " Gas Dispersion in Packed Beds", Chem. Eng. Sci. J., 23, 109-123.

Field, M.A., Gill,D.W., Morgan,B.B., and Hawksley,P.G.W. (1967), " Combustion of Pulverized Coal", Cheney & Sons Ltd., 322-325.

Gear, C.W. (1971), " The Automatic Integration of Ordinary Differential Equations", Communication of ACM, 1, 176.

Govind, R. and Shah, J. (1984), " Modeling and Simulation of an Entrained Flow Coal Gasifier", AIChE J., 3, 79.

Grens, E., and Thorsness, C. (1984), " Wall Recession Rates in Cavity-Growth Modeling ", Proc. 10th UCG Symp., Williamsburg, VA, 448.

Gunn, R.D. and Whitman, D.L. (1976), " An In Situ Gasification Model (Forward Mode) for Feasibility Studies and Design", Laramie Energy Research Center, Report LERC/RI-76/2.

Hindmarsh, A.C. (1980), " Two New Initial Value Ordinary Differential Equation Solvers", ACM Newsletter, 15, 10.

Johnson, S., and Hindmarsh, A. (1983), " Numerical Dynamic Simulation of Solid-Fluid Reactions in Isothermal Porous Spheres ", J. Comp. Phys., 52, 503-523.

Landau, H. (1950), " Heat Conduction in a Melting Solid ", Quart. Appl. Math., 8, 81-94.

Massaquoi, J., and Riggs, J. (1981), " Heat and Mass Transfer in a Burning Coal Seam ", Proc. 7th UCG Symp., 315-328.

Mondy, L., and Blottner, F. (1982), " The Drying of Coal in Underground Gasification ", Proc. 8th UCG symp., 355-364.

Olbrich, W.E., and Potter, O.E. (1972), " Mass Transfer from the Wall in Small Diameter Packed Beds", Chem. Eng. Sci., 27, 1733-1743.

Peters, N. (1979) " Premixed Burning in Diffusion Flames - The Flame Zone Model of Libby and Economos ", Int. J. Heat Mass Transfer, 22, 691-703.

Schlunder, E.U. (1978), " Transport Phenomena in Packed Bed Reactors", Ch.4 in Chemical Reaction Engineering-Houston, Luss, D., and Weekend, V., eds., Amer. Chem. Soc., ACS Symposium Series 72, Wash., D.C.

Sen Gupta, A., and Thodos, G. (1963), " Direct Analogy Between Mass and Heat Transfer to Beds of Spheres", AIChE J., 9, 751.

Sherwood, T., Pigford, R., and Wilke, C. (1975), Mass Transfer, McGraw-Hill Publish. Co., New York, 129-137.

Sohrab, S., Ye, Z., and Law, C. (1984), " Theory of Interactive Combustion of Counterflow Premixed Flames ", Spring Tech. Mtg. Western States of the Combustion Institute, Boulder, CO, 9.

Sincovec, R.F. and Madsen, N.K. (1975), " Software for Nonlinear Partial Differential Equations", ACM Transactions on Mathematical Software, 1, 232 .

Thorsness, C.B., Grens, E.A., and Sherwood, A.E. (1978), " A One-Dimensional Model for In Situ Coal Gasification", Lawrence Livermore National Laboratory, Report UCRL-52523.

Thorsness, C.B. and Cena, R.J. (1983), " An Underground Coal Gasification Cavity Simulator with Solid Motion", Lawrence Livermore National Laboratory, Report UCRL-89084.

Thorsness, C.B., and Kang, S-W. (1984), " A Method -Of-Line Approach to Solution of Packed-Bed Flow Problems Related to Underground Coal Gasification Processes", Proc. 10th Annual Underground Coal Gasification Symposium, Williamsburg, VA.

Wakao, N., and Kaguei, S. (1982), Heat and Mass Transfer in Packed Beds, Gordon and Breach Science Publ., New York.

Yagi, S., and Kunii, D. (1957), " Studies of Effective Thermal Conductivities in Packed Beds", AIChE J., 3, 373-381.

Yagi, S., and Wakao, N. (1959), " Heat ans Mass Transfer from Wall to Fluid in Packed Beds ", AIChE J., 5, 79-85.

Yoon, H., Wei, J., and Denn, M. (1978), " A Model for Moving Bed Gasification Reactors", AIChE J., 2, 885.

APPENDIX A. PARTICLE SIZE AND RELATED KINETIC PARAMETERS

Both the SP and AS kinetics models given in Eqs.(9) and (10) require several parameters to be calculated. These are the various particle diameters (d_p, d_u, and d_a), the particle number densities (N and N_a), the gas film mass transfer coefficient (k_c), the effective mass diffusivity inside a particle (D_e), and the effectiveness factor (η). Different relations are used for the particle sizes and number densities depending on the kinetic and solid motion assumptions made. For all assumptions the basic film coefficient and effectiveness factor relations are the same.

Mass and volume conservation in the packed bed has been used to determine these parameters. In particular, the following terms are introduced:

$$a = w_A^o(\rho_{II}/\rho_I); \quad b = (m_A/m_C)_o;$$

$$q = (1-\phi_o)/(1-\phi_e) \quad ; \quad Q = (1+b)F_4/\rho_{II}(1-\phi_o)$$

where the term w_A^o denotes the initial mass fraction of ash in the particle, I and II the the ash zone and the unreacted char+ash zone, respectively, b the original mass ratio of the ash and char, Q a measure of the char remaining in the unreacted portion of the particle, F_4 the carbon density in bed calculated from the GSF code as a part of the solution, and the subscript o the initial condition.

Case 1. Constant solid velocity (v_s = constant).

For the case of a zero solid velocity or constant imposed bed velocity and constant char-particle number density, the expressions for the particle size are:

SP model:

$$d_p = d_o \tag{A.1}$$

$$d_u = d_o\, Q^{1/3} \tag{A.2}$$

$$N = N_o = 6(1 - \phi_o)/[\pi d_o^3] \tag{A.3}$$

AS model:

$$d_p = d_u \tag{A.4}$$

$$d_u = d_o \, Q^{1/3} \tag{A.5}$$

$$d_A = f \, d_o \tag{A.6}$$

$$N = N_o = 6(1 - \phi_o)/[\pi d_o^3] \tag{A.7}$$

$$N_A = N \, [1/q - Q] \, / \, f^3 \tag{A.8}$$

Case 2. Constant bed -- $(1-\phi_e)\rho_s$ = constant.

The relations for the case in which the constant bed density assumption is made are however slightly more complicated. The equations for particle size and number density for the constant bed density assumption are the following.

SP model:

$$d_p = d_o \, [\, a \, / \, \{1-(1-a) \, q \, Q\}^{1/3}] \tag{A.9}$$

$$d_u = d_p \, (q \, Q)^{1/3} \tag{A.10}$$

$$N = 6(1 - \phi_e)/[\pi d_p^3] \tag{A.11}$$

AS model:

$$d_p = d_u \tag{A.12}$$

$$d_u = d_o \, [a \, q \, Q \, / \, \{1-(1-a) \, q \, Q\}]^{1/3} \tag{A.13}$$

$$d_A = f\, d_o \tag{A.14}$$

$$N = 6(1 - \phi_o)\, Q \,/\, [\pi d_u^3] \tag{A.15}$$

$$N_A = 6(1 - \phi_e)\, (1-qQ) \,/\, [\pi d_A^3] \tag{A.16}$$

Mass-transfer Coefficient (k_c).

Employing appropriate particle size from the above equations, we can obtain the external mass transfer coefficient used in the rate expressions. From Sen Gupta and Theodus (1963):

$$k_c = \frac{2.06\, g\, R\, T}{\epsilon\, P} (Sc)^{-0.092} \left(\frac{P\, D}{g\, R\, T\, d_p} \right)^{0.575} \tag{A.17}$$

Effectiveness Factor (η).

From Yoon et al. (1978) the effectiveness factor for the heterogeous reactions is given by

$$\eta = \frac{1}{\tau}\left[\frac{1}{\tanh(3\tau)} - \frac{1}{3\tau} \right] \tag{A.18}$$

where the term τ denotes Thiele modulus defined to be

$$\tau = \frac{d_p}{6} \sqrt{\frac{k_r\, \rho^*}{D_e}} \tag{A.19}$$

with the effective diffusivity approximated by $D_e = \phi_{int}\, D_m$.

In Eq.(A.19), the term ρ^* signifies the density of carbon in the unreacted particle, and the porosity ϕ_{int} used in the effective diffusivity is that of the unreacted particle. For the water-gas-shift reaction ρ^* is the total mass density of the ash (or unreacted particle), and corresponding ϕ_{int} is utilized to obtain the effective diffusivity.

APPENDIX B. TRANSPORT PROPERTIES

Various physical properties are needed in calculating the physico-chemical characteristics of a packed-bed flow. These properties are the viscosity and the specific heat of the gas, the thermal conductivity and the specific heat of the solid. For these four properties, we assume a linear change with temperature, i.e.,

$$F(T) = a + b\,T,$$

with prescribed a and b.

(1). Viscosity (gas).
In the present model we use; $a = 4\ (10^{-6})$ kg/m-K ;

$b = 2.93\ (10^{-8})$.

(2). Specific heat (gas).
We use: $a = 29.7$ J/mol-K ; $b = 1.2\ (10^{-2})$.

(3). Thermal conductivity (solid).
We use: $a = 10^{3}$ J/kg-K ; $b = 0$.

(4). Specific heat (solid).
We use: $a = 0.4$ W/m-K ; $b = 0$.

In addition, mass and thermal dispersions were found to take place in packed-bed flows (see, for example, Coberly and Marshall 1951, Deissler and Boegli 1958). These dispersions depend upon such physical factors as the porosity and the Reynolds number. We thus need to characterize these "effective" thermal and mass dispersion parameters.

Effective thermal dispersion coefficient (Perpendicular to flow direction).Here we use the empirical correlation of Wakao and Kaguei (1982; see also Yagi and Kunii 1957):

$$k_p^{eff}/k_g = k^0/k_g + 0.1\ Re\ Pr \qquad (B.1)$$

where the symbol k^{eff} denotes effective thermal "conductivity", Pr the Prandtl number, i.e., $Pr = \mu c_g/k_g$, k_g the gas thermal conductivity, Re the Reynolds number based upon the superficial velocity (U), and the particle diameter (d_p), i.e., $Re = Ud_p\rho/\mu$, and the subscript p the direction perpendicular to the flow direction. The term k^0 signifies effective" thermal conductivity (including the radiation effects) for the quiescent case, and expressed as:

$$k^0/k_g = \phi_e Nu_v + (1 - \phi_e)/\ [k_g/k_s + 1/(25 + Nu_s)] \qquad (B.2)$$

The "Nusselt" numbers for the vapor gas and the solid are defined to be:

$$Nu_v = (d_p/k_g)(0.2268)(T/100)^3/[\,1+\{\phi_e/(1-\phi_e)\}\,(1-\varepsilon)/(2\varepsilon)\,]$$

and $$Nu_s = (d_p/k_g)(0.2268)(T/100)^3\ [\varepsilon/(2 - \varepsilon)].$$

Figure B-1 shows sample behavior of the effective radial thermal dispersion, in this case as a function of temperature. The conditions used are Pr = 0.7, Sc = 0.6, Particle diameter = 0.025 m, Re = 87 (based on particle diameter), and the gas-mixture molecular weight = 0.0204 kg/mol. Note the increase of almost two decades at 1800 K from room temperature. This is mainly due to the radiative effects becoming dominant at temperatures above 1300 K.

Effective thermal dispersion coefficient (flow direction).
For the expression for the effective thermal conductivity in the axial direction, we use that obtained by Wakao and Kaguei (1982):

$$k_f^{eff}/k_g = k^0/k_g + 0.5\ Re\ Pr \qquad (B.3)$$

where the subscript f refers to the flow direction, and all other terms have been defined in Eq.(B.1). The magnitude changes with temperature are also

shown in Figure B-1. We observe that the relative magnitude between the axial and the radial thermal dispersions is small at high temperature, due largely to the radiative effects dominating in both directions.

Effective mass dispersion coefficient (Perpendicular to flow direction).Here we use the empirical correlation obtained by Bischoff (1969) for the effective radial mass dispersivity, expressed as :

$$D_p^{eff}/D_g = 0.73\,\phi_e + 0.1\ Re\ Sc \qquad (B.4)$$

and where the symbol D^{eff} denotes effective mass dispersion coefficient, Sc the Schmidt number defined to be the ratio of the kinematic viscosity and the molecular gas diffusivity (D_g), i.e., $Sc = \mu/\rho D_g$.

Figure B-2 shows typical behavior of the radial mass dispersion coefficient as a function of temperature. Relatively gradual increase in the value is seen with increasing temperature, unlike the effective thermal dispersion coefficients.

Effective mass dispersion coefficient (Flow direction).
For the axial coefficient we apply the correlation obtained by Edwards and Richardson (1968) :

$$D_f^{eff}/D_g = 0.73\,\phi_e + 0.5\ (Re\ Sc)^2/(9.7\,\phi_e + ReSc) \qquad (B.5)$$

where the terms have already been defined in Eq.(B.4). The variation of this coefficient with temperature is also shown in Figure B-2. Note that the effective dispersion coefficients retain their relatively large differences at all temperatures. This is in contrast to the effective thermal coefficients, for which the radiative effects become dominant at high temperatures.

APPENDIX C. NUMERICAL-SOLUTION PROCEDURES

In this section we describe in detail the procedures adopted in numerically solivng the partial differential equations by using a finite-difference method. First we give a generalized treatment of the numerical scheme used to express the PDE's. Second, we give specific descriptions of the various conservation equations.

C.1. Generalized Treatment of PDE's.

We note that the conservation equations given in Eqs.(1)-(6) share a common form, viz., they contain transient, gas and solid fluxes, diffusion, and source terms. Therefore, we consider a generic equation embodying these terms, and express it in a finite-difference form amenable to numerical solution.

The generalized partial differential equation is expressed in the form :

$$\frac{\partial A}{\partial t} = \frac{1}{b}[-\nabla.(\vec{fj} + \vec{gj_s} - a\nabla h) + S] \qquad (C.1)$$

where the term A denotes a dependent variable, a and b the multiplicative terms, f the flux for gas species, g the flux for solid phase, $\vec{j}$ and $\vec{j_s}$ the flux terms, h the diffusion, and S the source term. These terms contain the dependent variables of actual interest, such as the temperature, the species mole fraction, which can be determined once the PDE's have been solved.

In a rectangular coordinate system Eq.(C.1) can be written

$$\frac{\partial A}{\partial t} = \frac{1}{b}[-\frac{\partial}{\partial x}(fj^x + gj_s^x - a\frac{\partial h}{\partial x}) - \frac{\partial}{\partial y}(fj^y + gj_s^y - a\frac{\partial h}{\partial y}) + S] \qquad (C.2)$$

and for a cylindrical system we have : (x denoting the radial direction)

$$\frac{\partial A}{\partial t} = \frac{1}{b}[-\frac{1}{x}\frac{\partial}{\partial x}(xfj^x + xgj_s^x - ax\frac{\partial h}{\partial x}) - \frac{\partial}{\partial y}(fj^y + gj_s^y - a\frac{\partial h}{\partial y} + S] \qquad (C.3)$$

Now consider an interior node point at (M,N) shown in Fig. C.1.

The transient term $\partial A/\partial t$ is evaluated at node (M,N) such that $\partial A/\partial t = \partial A_{M,N}/\partial t$, and the multiplicative term b and the source term S are also evaluated at the node point (M,N).

The flux terms for the gases and the solids are of the same form, and can be expressed as follows.

$$\nabla.\vec{fj} = \frac{1}{\Omega_M \Delta x_M}[\Omega_{M+1/2}(f^* j^x)_{M+1/2,N} - \Omega_{M-1/2}(f^* j^x)_{M-1/2,N}]$$

$$+ \frac{1}{\Delta y_N}[(f^* j^y)_{M,N+1/2} - (f^* j^y)_{M,N-1/2}] \qquad (C.4)$$

where for a rectangular system $\Omega_{M+1/2,N} = \Omega_{M-1/2,N} = \Omega_{M,N} = 1$

and for a cylindrical system $\Omega_{M+1/2} = x_M^{ph}$; $\Omega_{M-1/2} = x_M^{lh}$; $\Omega_M = (x_M^{ph} + x_M^{lh})/2$.

Now the terms j are :

$j^x_{M+1/2,N}$: flux or velocity across the right boundary of of cell M,N ;

$j^x_{M-1/2,N}$: flux or velocity across the left boundary of cell M,N ;

$j^y_{M,N+1/2}$: flux or velocity across the top boundary of cell M,N ;

$j^y_{M,N-1/2}$: flux or velocity across the bottom boundary of cell M,N ;

and the functions f are :

$f^*_{M+1/2,N}$: f evaluated at node M,N for $j^x_{M+1/2,N}>0$, and at node M+1,N for $j^x_{M+1/2,N}<0$;

$f^*_{M-1/2,N}$: f evaluated at node M-1,N for $j^x_{M-1/2,N}>0$, and at node M,N for $j^x_{M-1/2,N}<0$;

$f^*_{M,N+1/2}$: f evaluated at node M,N for $j^y_{M,N+1/2}>0$, and at node M,N+1 for $j^y_{M,N+1/2}<0$;

$f^*_{M,N-1/2}$: f evaluated at node M,N-1 for $j^y_{M,N-1/2}>0$, and at node M,N for $j^y_{M,N-1/2}<0$;

The diffusion term is expressed as :

$$\nabla.(a\nabla h) = \frac{1}{\Omega_M \Delta x_M}\left[\Omega_{M+1/2}\left(a\frac{\partial h}{\partial x}\right)_{M+1/2,N} - \Omega_{M-1/2}\left(a\frac{\partial h}{\partial x}\right)_{M-1/2,N}\right] + \frac{1}{\Delta y_N}\left[\left(a\frac{\partial h}{\partial y}\right)_{M,N+1/2} - \left(a\frac{\partial h}{\partial y}\right)_{M,N-1/2}\right]$$

where

$$\left(a\frac{\partial h}{\partial x}\right)_{M+1/2,N} = a_{M+1/2,N}\frac{h_{M+1,N} - h_{M,N}}{x_{M+1} - x_M}$$

$$\left(a\frac{\partial h}{\partial x}\right)_{M-1/2,N} = a_{M-1/2,N}\frac{h_{M,N} - h_{M-1,N}}{x_M - x_{M-1}}$$

$$(a\frac{\partial h}{\partial y})_{M,N+1/2} = a_{M,N+1/2}\frac{(h_{M,N+1} - h_{M,N})}{(y_{N+1} - y_N)}$$

$$(a\frac{\partial h}{\partial y})_{M,N-1/2} = a_{M,N-1/2}\frac{(h_{M,N} - h_{M,N-1})}{(y_N - y_{N-1})}$$

and

$a_{M+1/2,N}$: a evaluated at right boundary of cell M,N ;

$a_{M-1/2,N}$: a evaluated at left boundary of cell M,N ;

$a_{M,N+1/2}$: a evaluated at upper boundary of cell M,N ;

$a_{M,N-1/2}$: a evaluated at lower boundary of cell M,N .

C.2. Boundary Conditions.

The boundary conditions are applied at boundary cells by formally integrating across the boundary to obtain the following general form (applied at M=1 or at M=n_x) :

$$(\frac{\partial A}{\partial t})_{M,N} = \frac{1}{b\Delta x_M}\,[\,\frac{1}{\Omega_M}[\,-\Omega_{M+1/2}(f^* j^x)_{M+1/2,N} + \Omega_{M-1/2}(f^* j^x)_{M-1/2,N}$$
$$- \Omega_{M+1/2}(g^* j_s^x)_{M+1/2,N} + \Omega_{M-1/2}(g^* j^x)_{M-1/2,N}$$
$$+ (a\Omega\frac{\partial h}{\partial x})_{M+1/2,N} - (a\Omega\frac{\partial h}{\partial x})_{M-1/2,N}\,]$$

$$+ \Delta x_M[\,-(\frac{\partial(fj^y)}{\partial y})_{M,N} - (\frac{\partial(gj_s^y)}{\partial y})_{M,N} + (\frac{\partial}{\partial y}a\frac{\partial h}{\partial y})_{M,N} + S_{M,N}\,]\,]$$

where the $f\,j^x$ and $g\,j_s^x$ terms are defined as in the previous development at the interior boundary and are given by the conditions at the exterior boundary.
The $f\,j^y$ and $g\,j_s^y$ terms are similar and are given by the form :

$$(\frac{\partial}{\partial y}(fj^y))_{M,N} = \frac{1}{\Delta y_N}[\,(f^* j^y)_{M,N+1/2} - (f^* j^y)_{M,N-1/2}\,]$$

Terms on the right are defined as previously given.

The $a\frac{\partial h}{\partial x}$ terms are defined as in the previous development at the interior boundary and are given by the conditions at the exterior boundary. Finally we have :

$$[\frac{\partial}{\partial y}(a\frac{\partial h}{\partial y})]_{M,N} = \frac{1}{\Delta y_N}[\,(a\frac{\partial h}{\partial y})_{M,N+1/2} - (a\frac{\partial h}{\partial y})_{M,N-1/2}\,]$$

Terms on the right are defined as previously given.

The $\partial h/\partial x$ terms at the outer boundary are found by invoking flux continuity there, i.e., $flux^- = flux^+$, where the signs + and - refer to values just inside and outside the boundary, respectively.

For the right-hand boundary :

$$flux^- = (f^* j^x)_{n_x+1/2,N} + (g^* j_s^x)_{n_x+1/2,N} - (a\frac{\partial h}{\partial x})_{n_x+1/2,N};$$

$flux^+$ = given by boundary conditions.

For the left-hand boundary :

$flux^-$ = given by boundary conditions.

$$flux^+ = (f^* j^x)_{1-1/2,N} + (g^* j_s^x)_{1-1/2,N} - (a\frac{\partial h}{\partial x})_{1-1/2,N}$$

For the bottom (or top) boundary (N=1 or N=n_y) :

$$(\frac{\partial A}{\partial t})_{M,N} = \frac{1}{b\Delta y_N}[-(f^* j^y)_{M,N+1/2} + (f^* j^y)_{M,N-1/2} - (g^* j_s^y)_{M,N+1/2} + (g^* j_s^y)_{M,N-1/2}$$
$$+ (a\frac{\partial h}{\partial y})_{M,N+1/2} - (a\frac{\partial h}{\partial y})_{M,N-1/2}$$
$$+ \Delta y_N[-\frac{1}{\Omega_M}\frac{\partial}{\partial x}(\Omega f j^x)_{M,N} - \frac{1}{\Omega_M}\frac{\partial}{\partial x}(\Omega g j_s^x)_{M,N}$$
$$+ \frac{1}{\Omega_M}(\frac{\partial}{\partial x}a\Omega\frac{\partial h}{\partial x})_{M,N} + S_{M,N}]]$$

where the fj^y and gj_s^y terms are defined as in the previous development at the interior boundary and are given by conditions at the exterior boundary. The fj_x and gj_s^x terms are similar and are given by the form :

$$[\frac{\partial}{\partial x}(\Omega f^* j^x)]_{M,N} = \frac{1}{\Delta x_M}[\Omega_{M+1/2}(f^* j^x)_{M+1/2,N} - \Omega_{M-1/2}(f^* j^x)_{M-1/2,N}]$$

Terms on the right are defined as previously given. The $a\partial h/\partial y$ terms are defined as in the previous development at the interior boundary and are given by conditions at the exterior boundary. Finally,

$$(\frac{\partial}{\partial x}a\Omega\frac{\partial h}{\partial x})_{M,N} = \frac{1}{\Delta y_N}[(\Omega a\frac{\partial h}{\partial x})_{M+1/2,N} - (\Omega a\frac{\partial h}{\partial x})_{M-1/2,N}]$$

Terms on the right are defined as previously given.

The $\partial h/\partial y$ terms at the outer boundary are found by invoking flux continuity at the outer boundary.

For the top boundary :

$$flux^- = (f^* j^y)_{M,n_y+1/2} + (g^* j_s^y)_{M,n_y+1/2} - (a\frac{\partial h}{\partial y})_{M,n_y+1/2};$$

flux$^+$: given by boundary conditions.

For the bottom boundary :

flux$^-$: given by boundary conditions.

$$\text{flux}^+ = (f^+ j^y)_{M,1-1/2} + (g^+ j_g^y)_{M,1-1/2} - (a\frac{\partial h}{\partial y})_{M,1-1/2}$$

C.3. Specific Descriptions of Conservation Equations.

Now that finite-difference forms have been developed for a generic PDE in the previous section, we proceed to describe some specific forms relevant to each conservation equation.

C.3.1. Overall Gas Balance: Eq.(1).

In terms of Eq.(C.1), we have :

$A = \phi C$
$b = 1$
$f = \phi C = A$
$\vec{j} = \vec{v}$
$g = 0$

$\vec{j}_s = 0$
$a = 0$
$h = 0$
$S = \sum_{i=1}^{n} Q_i + \sum_{i=1}^{n} s_i$, which yields

$$\frac{\partial}{\partial t}(\phi C) = -\nabla.(\phi C\vec{v}) + \sum_{i=1}^{n} Q_i + s_i$$

that is, Eq.(1). Here the term $(Q_i)_{M,N}$ denotes the gas species introduced along the wall (where appropriate), $(s_i)_{M,N}$ the source terms arising from reactions taking place in the cell, given by ;

$$s_i = \sum_{j=1}^{n} \alpha_{ij}\, r_j$$

where α_{ij} is the stoichiometric coefficient for gas species i in reaction j, and r_j is the rate of reaction j per unit volume of bed.

The velocity vector $\vec{v}$ used in this equation and elsewhere is obtained from the variable ϕC by as follows. The velocity is composed of x and y components whose values are defined at cell boundaries. These velocities are based on the ideal-gas and the Darcy laws, i.e.,

Ideal gas law $C = \frac{P}{RT}$;

Darcy law $\vec{U} = -\frac{\Gamma}{\mu}\nabla P$.

First the pressure is determined from

$$P_{M,N} = (\phi C)_{M,N} T_{M,N} R \frac{1}{\phi_{M,N}}$$

We now introduce the term mobility β for a given cell defined as

$$\beta_{M,N} = \frac{\Gamma_{M,N}}{(\mu)_{T_{M,N}}}$$

To calculate the velocity in the cells we need to evaluate the mobilities across interfaces. For simplicity a straight arithmetic average is chosen here. The notation 1/2 signifies interface values.

$$\beta_{M+1/2,N} = \frac{\beta_{M,N} + \beta_{M+1,N}}{2}$$

$$\beta_{M,N+1/2} = \frac{\beta_{M,N} + \beta_{M,N+1}}{2}$$

The true gas velocities are then obtained by using Darcy's law and the relation : $\phi\vec{v} = \vec{U}$.

$$v^x_{M+1/2,N} = \frac{\beta_{M+1/2,N} (P_{M,N} - P_{M+1,N})}{\phi^*_{M+1/2,N} (x_{M+1} - x_M)}$$

$$v^y_{M,N+1/2} = \frac{\beta_{M,N+1/2} (P_{M,N} - P_{M,N+1})}{\phi^*_{M,N+1/2} (x_{M+1} - x_M)}$$

The superscripts on the velocity terms denote the x and y directions.

For consistency with the upwind defference scheme used in conservation equations, the appropriate porosities ϕ used above are defined as

$$\phi^*_{M+1/2,N} = \phi_{M,N} \quad \text{for} \quad v^x_{M+1/2,N} > 0;$$

$$\phi_{M+1,N} \quad \text{for} \quad v^x_{M+1/2,N} < 0;$$

$$\phi^*_{M,N+1/2} = \phi_{M,N} \quad \text{for} \quad v^y_{M,N+1/2} > 0;$$

$$\phi_{M,N+1} \quad \text{for} \quad v^y_{M,N+1/2} < 0;$$

These reactions are for the right and upper boundaries of each cell. Those for the left and lower boundaries are obtained >from the above by decrementing M or N by one.

Boundary Conditions :

For outflow condition, we usually prescribe the value of the exit pressure across the top boundary. However, we use the following :

$$v^y_{M,n_y+1/2} = \beta_{M,n_y} \Theta \frac{(P_{M,n_y} - P_{out})}{(y_{n_y} - y_{n_y-1})}$$

Here Θ is a large positive number (~ 100) and the y distance is included to retain proper length scaling. This approach results in P_{M,n_y} being set very nearly equal to P_{out} , and is utilized here to maintain the

conservative nature of the gas flow.

At the inflow boundary nodes located at the bottom of the system, we have :

$$(f^* j^y)_{M,1-1/2} = ((\phi C)^* v^y)_{M,1-1/2} = \sum_{i=1}^{n} F_i$$

where F_i are the injection rates per unit inflow area of gas species i. Note that this formulation is equivalent to setting $v^y = 0$ at the bottom and treating the inflow as a source term, like Q_i , after multiplying F_i by the area/volume ratio of the injection cell to put the inflow on a per unit volume basis.

At all other boundaries, a no-flow condition is invoked by setting to zero the $\phi C\vec{v}$ evaluated at these oundaries.

The true gas velocities are then obtained by using Darcy's law and the relation : $\phi\vec{v} = \vec{U}$.

$$v^x_{M+1/2,N} = \frac{\beta_{M+1/2,N}\,(P_{M,N} - P_{M+1,N})}{\phi^*_{M+1/2,N}\,(x_{M+1} - x_M)}$$

$$v^y_{M,N+1/2} = \frac{\beta_{M,N+1/2}\,(P_{M,N} - P_{M,N+1})}{\phi^*_{M,N+1/2}\,(x_{M+1} - x_M)}$$

The superscripts on the velocity terms denote the x and y directions.

For consistency with the upwind defference scheme used in conservation equations, the appropriate porosities ϕ used above are defined as

$$\phi^*_{M+1/2,N} = \phi_{M,N} \quad \text{for} \quad v^x_{M+1/2,N} > 0;$$

$$\phi_{M+1,N} \quad \text{for} \quad v^x_{M+1/2,N} < 0;$$

$$\phi^*_{M,N+1/2} = \phi_{M,N} \quad \text{for} \quad v^y_{M,N+1/2} > 0;$$

$$\phi_{M,N+1} \quad \text{for} \quad v^y_{M,N+1/2} < 0;$$

These reactions are for the right and upper boundaries of each cell. Those for the left and lower boundaries are obtained >from the above by decrementing M or N by one.

Boundary Conditions :

For outflow condition, we usually prescribe the value of the exit pressure across the top boundary. However, we use the following :

$$v^y_{M,n_y+1/2} = \beta_{M,n_y}\Theta\frac{(P_{M,n_y} - P_{out})}{(y_{n_y} - y_{n_y-1})}$$

Here Θ is a large positive number (~ 100) and the y distance is included to retain proper length scaling. This approach results in P_{M,n_y} being set very nearly equal to P_{out} , and is utilized here to maintain the conservative nature of the gas flow.

At the inflow boundary nodes located at the bottom of the system, we have :

$$(f^* j^y)_{M,1-1/2} = ((\phi C)^* v^y)_{M,1-1/2} = \sum_{i=1}^{n} F_i$$

where F_i are the injection rates per unit inflow area of gas species i. Note that this formulation is equivalent to setting $v^y = 0$ at the bottom and treating the inflow as a source term, like Q_i , after multiplying F_i by the area/volume ratio of the injection cell to put the inflow on a per unit volume basis.

At all other boundaries, a no-flow condition is invoked by setting to zero the $\phi C\vec{\nabla}$ evaluated at these boundaries.

C.3.2. Gas Species Conservation: Eq.(2).

Here we have $A = \phi c_i$;
$b = 1$;
$\underline{f} = \phi c_i = A$;
$\vec{j} = \vec{\nabla}$;
$\underline{g} = 0$;
$\vec{j}_g = 0$;
$a = CD$;
$h = y_i$;
$S = Q_i$.

Substitution of these terms in Eq.(C.1) yields

$$\frac{\partial}{\partial t}(\phi c_i) = -\nabla.(\phi c_i \vec{\nabla} + CD\nabla y_i) + Q_i + s_i$$

which is Eq.(2), as expected. The terms Q_i and s_i are gas-source terms, and $\vec{\nabla}$ term is the true gas velocity as previously defined.

Now

$$a_{M+1/2,N} = C_{M+1/2,N} D_{M+1/2,N},$$

where

$$C_{M+1/2,N} = 0.5 \left[\frac{(\phi C)_{M,N}}{\phi_{M,N}} + \frac{(\phi C)_{M+1,N}}{\phi_{M+1,N}}\right]$$

$D_{M+1/2,N}$ = Mass dispersion coefficient at the right-cell boundary. Its magnitude is obtained by using correlation described in Appendix B and the following dependent variables :

$C_{M+1/2,N}$: previously defined ;

$T_{M+1/2,N}$, $(\phi_e)_{M+1/2,N}$, $\phi_{M+1/2,N}$, $(d_p)_{M+1/2,N}$, $(N_A)_{M+1/2,N}$, $N_{M+1/2,N}$, $\omega_{M+1/2,N}$

all defined by simple average of M,N and M+1,N values. Here ω is gas molecular weight expressed as kg/mol.

Also,

$$(\mu)_{M+1/2,N} = 0.5 \left[(\mu)_{T_{M,N}} + (\mu)_{T_{M+1,N}} \right]; \quad (c_p)_{M+1/2,N} = 0.5[(c_p)_{T_{M,N}} + (c_p)_{T_{M+1,N}}];$$

$\vec{\nabla}$ = given by $v^x_{M+1/2,N}\, \vec{e}_x + v^y_{M+1/2,N}\, \vec{e}_y$,

wher $v^x_{M+1/2,N}$ is given as previously defined, and $v^y_{M+1/2,N}$ is obtained >from the following average :

$$v^y_{M+1/2,N} = 0.25[\, v^y_{M,N+1/2} + v^y_{M,N-1/2} + v^y_{M+1,N+1/2} + v^y_{M+1,N-1/2}\,]$$

$D_{M,N+1/2}$ = Mass dispersion coefficient at the top cell boundary. The values used in the correlation are obtained in a manner completely analogous to those for the $D_{M+1/2,N}$ coefficient except the roles of M and N are reversed.

Boundary conditions :

For outflow or top boundary, we have :

$$\text{flux}^- = [(\phi c_i)^* v^y]_{M,n_y+1/2} - (CD\frac{\partial y_i}{\partial y})_{M,n_y+1/2}$$

$$\text{flux}^+ = [(\phi c_i)^* v^y]_{M,n_y+1/2} .$$

This results in $(\frac{\partial y_i}{\partial y})_{M,n_y+1/2} = 0$.

For inflow or bottom boundary :

$$\text{flux}^- = (F_i)_{x_w}$$

$$\text{flux}^+ = [(\phi c_i)^* v^y]_{M,1-1/2} - (CD\frac{\partial y_i}{\partial y})_{M,1-1/2}$$

This then results in :

$$(\frac{\partial y_i}{\partial y})_{M,1-1/2} = \frac{1}{(CD)_{M,1-1/2}} [\, (\phi c_i)_{M,1}\, v^y_{M,1-1/2} - (F_i)_{x_w} \,]$$

For cases in which $F_i = 0$, $v_{M,1-1/2}$ is taken as zero, yielding $(\frac{\partial y_i}{\partial y})_{M,1-1/2} = 0$.

Side boundaries :

Both side boundaries are taken as no-flow boundaries and therefore we have

$$(\frac{\partial y_i}{\partial x})_{\text{boundary}} = 0.$$

C.3.3. Solid Species Conservation: Eq.(3).

We have :

$A = (1-\phi_e)\rho_s\omega_k$
$b = 1$
$f = 0$
$\vec{j} = 0$
$g = (1-\phi_e)\rho_s\omega_k = A$

$\vec{j}_s = \vec{v}_s$
$a = 0$
$h = 0$
$S = S_k^*$

These terms in Eq.(C.1) yields

$$\frac{\partial}{\partial t}[1-(\phi_o)\rho_s\omega_k] = -\nabla.[(1-\phi_o)\rho_s\omega_k\vec{v}_s] + S_k^*$$

which is Eq.(3), as expected. We now describe these terms.

$(S_k^*)_{M,N}$ = solid source terms arising from reactions taking place in the cell, and is expressed as

$$S_k^* = \sum_{j=1}^{n} \alpha_{jk}^* r_j$$

where α_{jk}^* is the stoichiometric coefficient in appropriate units (kg/mol of reaction) for solid species k in reaction j.

$(v_s^x)_{M+1/2,N}$: Solid velocity in x-direction is always zero.

$(v_s^y)_{M,N+1/2}$: Solid velocities in the vertical direction at the cell-top boundary. This is obtained from one of two different relations depending on the assumed physics, i.e.,

Assumption 1 : Constant solid velocity.
The velocity is prescribed as a fixed value, including the zero solid-motion case with $v_s^y=0$.

Assumption 2 : Constant bed density.
Here the local solid velocity is obtained by Eq.(8). In discretized form this becomes

$$(v_s^y)_{M,N+1/2} = (v_s^y)_{M,N-1/2} + \Delta y_N \frac{(\sum_{k=1}^{m} s_k^*)_{M,N}}{\rho_s},$$

with $(v_s^y)_{M,N1-1/2} = (v_s)_o$.

Boundary conditions :

Along the top boundary the inflow (solid) composition is set equal to given values, i.e.,

$$(gj_s^y)_{M,n_y+1/2} = (1-\phi_o)(\rho_s)_o(\omega_k)_o(v_s^y)_{M,n_y+1/2}$$

where $(\omega_k)_o$ is the input weight fraction of solid species " k ".

Along the bottom boundary the solid composition at the boundary node is used in the outflow term, i.e.,

$$(g_i\vec{j}')_{M,1-1/2} = [\,(1-\phi_e)\rho_s\omega_k)_{M,1}(v_s^x)_{M,1-1/2}$$

No special condition need be applied at the side boundaries, since v_s^x is taken as zero everywhere.

C.3.4. Energy Conservation: Eq.(5).

We have :

$A = T$

$b = \phi c_p \sum_{i=1}^{n} c_i + (1-\phi_e)\rho_s c_s \sum_{k=1}^{m} \omega_k$

$f = h_i$

$\vec{j} = \vec{j}_i$ and summed over i=1,n

$g = (1-\phi_e)\rho_s \sum_{k=1}^{m} (\omega_k h_k^*)$

$\vec{j}_s = \vec{v}_s$

$a = k$

$h = T = A$

Bacause the temperature T is a property of interest, we rewrite Eq.(5) to obtain explicitly the time derivate of T:

$$\frac{\partial T}{\partial t} = \frac{1}{[\phi c_p \sum_{i=1}^{n} c_i + (1-\phi_e)\rho_s c_s]} [-\nabla.[\sum_{i=1}^{n} (h_i \vec{j}_i) + \vec{v}_s(1-\phi_e)\rho_s \sum_{k=1}^{m} (\omega_k h_k^*) - k\nabla T\,] + W\,]$$

with $\vec{j}_i = \phi c_i \vec{v} - CD\nabla y_i$

As for $(1-\phi_e)\rho_s$: The solid-bed density is obtained in one of two ways, depending on the physical assumptions made. This is coupled directly to the previous assumptions related to the solid velocity.

Assumption 1 : Constant solid velocity.
This now implies variable solid density, i.e.,

$$(1-\phi_e)(\rho_s)_{M,N} = \frac{\sum_{k=1}^{m} [(1-\phi_e)\rho_s\omega_k]}{(\phi_e)_{M,N}}$$

Assumption 2 : Constant bed density.
This condition gives

$$(1-\phi_e)(\rho_s)_{M,N} = [\,(1-\phi_e)\rho_s]_o$$

where the right-hand-side denotes the initial bed density.

$k_{M+1/2,N}$: Effective bed thermal conductivity at the right cell boundary obtained using the correlations

described in Appendix B. The required dependent variables are defined in the same manner as those previously given for the dispersion coefficient $D_{M+1/2,-1}$.

$k_{M,N+1/2}$: Effective bed thermal conductivity at the top cell boundary. The values used in the correlations are obtained in the same manner as those for the dispersion coefficient $D_{M,N+1/2}$.

Boundary conditions :

Although a variety of conditions can be imposed on the thermal equation, two regions are always handled the same way. These are the left-side (or symmetry) plane and the injection nodes.

The symmetry plane : Here M=1, and the temperature gradient is set to zero, as is the flux term, i.e.,

$$(\frac{\partial T}{\partial x})_{1-1/2,N} = 0 :$$

$$(f^* j_x)_{1-1/2,N} = (\sum_{i=1}^{n} h_i j_i v^x)_{1-1/2,N} = 0 .$$

The injection node : This is located at the bottom plane, N=1. We invoke the continuity condition ;

$$\text{flux}^- = (\sum_{i=1}^{n} F_i h_i)_{T_{in}} + [\,(v_g^y)_o (1-\phi_e)\rho_s \sum_{k=1}^{m} \omega_k h_k^*\,]_{T_{in,1}}$$

$$\text{flux}^+ = (\sum_{i=1}^{n} h_i j_i^y)_{M,1-1/2} + [(v_g^y)(1-\phi_e)\rho_s \sum_{k=1}^{m} \omega_k h_k^*\,]_{M,1-1/2} - k_{M,1-1/2}(\frac{\partial T}{\partial y})_{M,1-1/2}$$

Since the solids are assumed to leave at the same temperature as the bottom cell, the solid term vanishes, and the above relation is solved for the temperature-gradient term :

$$(\frac{\partial T}{\partial y})_{M,1-1/2} = \frac{1}{k_{M,1-1/2}} [\,(\sum_{i=1}^{n} h_i j_i^y)_{M,1-1/2} - \sum_{i=1}^{n} F_i h_i\,]$$

Top (outflow) cells : Two different types of conditions are applied, i.e., zero conduction and radiant heat transfer. Both of these cases are handled by invoking an energy-flux continuity condition at the outflow plane ;

$$\text{flux}^- = (\sum_{i=1}^{n} h_i\, j_i^y\,)_{M,n_y+1/2} + [\,v_g^y\,(1-\phi_e)\,\rho_s \sum_{k=1}^{m} \omega_k\, h_k^*\,]_{M,n_y+1/2} - k_{M,n_y+1/2}\,(\frac{\partial T}{\partial y})_{M,n_y+1/2} \;;$$

$$\text{flux}^+ = (\sum_{i=1}^{n} h_i\, j_i^y\,)_{M,n_y+1/2} + (\,v_g^y)_{M,n_y+1/2}\,(1-\phi_{eo})\,\rho_o \sum_{k=1}^{m} \omega_{ko}\,(h_k^*)_{T_{\infty}} + S\,(\,T_{M,n_y}^4 - T_{\infty}^4\,)$$

Therefore, we have :

$$(\frac{\partial T}{\partial y})_{M,n_y+1/2} = \frac{1}{k_{M,n_y+1/2}} \;[\;[\,v_g^y\,(1-\phi_e)\,\rho_s \sum_{k=1}^{m} \omega_k\, h_k^*\,]_{M,n_y+1/2}$$

$$- (v_g^y)_{M,n_y+1/2} (1-\phi_{so}) \rho_o \sum_{k=1}^{m} \omega_{ko} (h_k^*)_{T_{s,o}} - S (T_{M,n_y}^4 - T_\infty^4)]$$

For the zero-radiant transport case, S = 0, and the last term in the temperature-gradient expression vanishes.

Right-side (wall) cells :

Three different types of boundary conditions are applied here : (1) adiabatic ; (2) wall heat transfer ; (3) wall heat transfer coupled to wall drying/pyrolysis.

All of these conditions are handled by invoking energy-flux conservation at the center boundary, i.e.,

$$\text{flux}^- = - k_{n_x+1/2,N} (\frac{\partial T}{\partial x})_{n_x+1/2,N} ;$$

$$\text{flux}^+ = h_w (T_{n_x,N} - T_w) + Q_D .$$

Therefore, we have :

$$(\frac{\partial T}{\partial x})_{n_x+1/2,N} = - \frac{1}{k_{n_x+1/2,N}} [h_w (T_{n_x,N} - T_w) + Q_D].$$

Here Q_D is a heat load associated with wall drying and pyrolysis and has been defined earlier.
For the adiabatic case, $h_w = 0$ and $Q_D = 0$.
For the wall heat- transfer case, $Q_D = 0$. In practice the heat-load term Q_D is used as a heat-sink term W in the equations by putting it on a per unit volume basis.

Bottom, non-inflow cells : The same three conditions used for the wall cells can be applied along these bottom cells which are not injection cells, and are handled in a completely analogous manner.

$$\text{flux}^- = h_w (T_{M,1} - T_w) + Q_D .$$

$$\text{flux}^+ = - k_{M,1+1/2} (\frac{\partial T}{\partial x})_{M,1+1/2}$$

Therefore, we have :

$$(\frac{\partial T}{\partial x})_{M,1+1/2} = - \frac{1}{k_{M,1+1/2}} [h_w (T_{M,1} - T_w) + Q_D].$$

APPENDIX D. WALL RECESSION-RATE MODEL

(This is based on the heat-transfer model developed by Grens and Thorsness 1984).

The wall recession-rate model represents the situation shown in Figure D.1, where the coordinate Z moves along the recession of the cavity wall with velocity u. Although this is not a steady-state process, the transient terms arising in heat transport into the wet coal (Landau 1950) have little effect on the time scale of coal gasification and can be ignored (Mondy and Blottner 1982). Thus the process is considered in the quasi-steady state, and the drying front ($T = T_d$) remains at a constant distance ξ from the cavity wall ($T = T_f$). At the wall the dried/pyrolyzed coal degrades to rubble by thermo-mechanical failure with no heat effect, and at the drying front the net heat flux must provide heat to dry the coal at the rate of davance of front u.

Under these conditions, with negligible heat of pyrolysis, all heat fluxes involved must be equal and constant, these heat fluxes being to the wall from the bed (Q_f), through the wall layer (Q), and at the drying front (Q_d), i.e.,

$$Q_f = Q = Q_d = u \rho^o H_v f_w \qquad (D.1)$$

where ρ^o is the density of the wel coal, H_v the heat of vaporization of the water in the coal, and f_w is the mass fraction of the water. Then, if the char-failure temperature is specified, the wall recession rate (u) can be determined directly by the convective heat transfer from the bed to the wall.

D.1. Heat Transfer to Wall of Char Bed.

The transfer of heat to the walls of packed beds has been extensively studied and reasonably well characterized except for cases of very low Reynolds numbers or high solid-particle conductivities (Dixon and Cresswell 1979); neither obtains here. The correlation of Yagi and Wakao (1959) provides a good representation of heat transfer coefficient (h) to the wall:

$$\frac{h}{c_g V} Pr^{2/3} = \begin{cases} 0.6\,Re^{1/2} & (Re < 40)\,; \\ 0.2\,Re^{-0.2} & (Re > 40)\,, \end{cases} \qquad (D.2)$$

where Pr is the Prandtl number in the bed, Re the Reynolds number defined to be $\rho d_p V/\mu$, c_g the gas heat capacity, μ the viscosity, and d_p the effective diameter of bed particles. The values of h given by this correlation are in good agreement with those found by Calderbank and Pogorsky (1957) at high Reynolds numbers.

However, the heat-transfer coefficient given by the above correlation must be corrected by the effect of high adverse mass flux from the wall during cavity growth. This flux arises in the flow of water vapor and pyrolysis gases from the wall (and by wall movement), and serves to reduce thermal gradients in the bed near the wall. It thus leads to lower heat-transfer coefficients than would be found in the absence of such flux. The correction for high mass flux is not sensitive to the model for heat transfer at the wall; corrections based on simple film models are adequate. Such a correction based on the treatment of Colburn and Drew (1937) can be expressed in the form :

$$\frac{h^o}{h} = \frac{\ln(1+\Omega)}{\Omega} \qquad (D.3)$$

where

$$\Omega = \frac{u\rho^o c_m (T_b - T_f)}{Q_f + u\rho^o c_m (T_f - T_d)} = \frac{(T_b - T_f)}{\theta^* + (T_f - T_d)}$$

The term h^o denotes the heat-transfer coefficient corrected for high mass flux, $\theta^* = H_v f_w / c_m$, Ω the ratio of the heat carried by the mass flux into the bed to the gross heat flux to the wall by the convective mechanism, and c_m the effective heat capacity of the material passing through the wall, represented by

$$c_m = f_w c_w + f_g c_g + f_s c_s \qquad (D.4)$$

the subscripts g ans s denoting the pyrolysis gas and the solid material, respectively.

Now the corrected heat-transfer coefficient can be used to calculate Q_f in Eq.(D.1);

$$Q_f = h^o(T_b - T_f) - u\,\rho^o c_m (T_f - T_d) = u\,\rho^o c_m f_w \qquad (D.5)$$

This expression is then solved for the recession rate, which is the velocity u at the wall:

$$u\rho^o c_m = \frac{h^o(T_b - T_f)}{\theta^* + (T_f - T_d)} = h^o \Omega = h \ln(1+\Omega) \qquad (D.6)$$

and therefore

$$u = \frac{h}{c_m \rho^o} \ln(1+\Omega) \qquad (D.7)$$

If the wall temperature is high enough for gasification reactions to occur, this model can still provide wall recession rates, assuming that adequate amount of steam is present to gasify the char at the wall at its heat-transfer-limited rate; usually only little steam must be supplied from the bed for this condition to obtain. The wall temperature is set such that C/H_2O reaction becomes fast, and the value of H_v is increased to account for the endothermic heat of gasification of the char at the wall.

The results of this heat-transfer calculation do not involve any detailed description of the phenomena in the wall layer, only the characteristic that, for a constant heat flux to the wall, the wall recedes at a constant velocity in the quasi-steady state. If the thermo-mechanical behavior of the wall is characterized by a breakdown temperature (T_f is specified), this is all that is required for the wall recession-rate representation. If the wall-behavior is parameterized by a failure thickness (ξ is specified), an examination of transport in the wall layer is necessary.

D.2. Heat Transfer in the Dried/Pyrolyzed Coal Layer.

The wall layer thickness ξ, the wall temperature T_f, and the recession rate u are related by transport (and other) mechanisms in the wall layer. Here these are considered in a greatly simplified form and at the quasi-state state; this is appropriate for representing the thermo-mechanical behavior by a single failure thickness. A more comprehensive examination of these mechanisms at the quasi-state state has been presented by Massaquoi and Riggs (1981).

For the present treatment we assume constant effective thermal conductivity k and constant overall heat capacity c_m (as defined in Eq.(D.4)) in the layer, negligible heat of pyrolysis, no gasification reactions, and isobaric conditions. Then the heat flux Q in the layer for Eq.(D.1) is given by

$$Q = -k\,dT/dZ - u\,\rho^{o} c_m (T-T_d) = u\,\rho^{o} H_v f_w \qquad (D.8)$$

with the boundary conditions

$$Z = 0 : \quad T = T_f ;$$
$$Z = \xi : \quad T = T_d$$

Equation(D.8) is recast in the nondimensional form

$$d\psi/d\zeta + \psi = -S \qquad (D.9)$$

with the boundary conditions

$$\zeta = 0: \qquad \psi = 1;$$

$$\zeta = (u \rho^{o} c_m \xi)/k: \qquad \psi = 0$$

where $\psi=(T-T_d)/(T_f-T_d)$, $\zeta=(u \rho^{o} c_m Z)/k$, and

$$S=(H_v f_w)/[c_m(T_f-T_d)].$$

Equation (9) has the solution:

$$\psi = -S + (1 + S) \exp(-\zeta) \tag{D.10}$$

with the eigenvalue requirement on u:

$$u=\frac{k}{c_m \rho^{o} \xi} \ln(1+\frac{1}{S}) \tag{D.11}$$

Equations (7) and (11) can be solved simultaneously for T_f, and then either equation can be used to determine the wall recession rate u.

Having obtained the wall-regression rate u, we can now calculate the species-production rates as follows.

$$s_i = u c_i \frac{\rho_w - (1-\phi_s)\rho_2}{V_{rx} \Delta_r} \tag{D.12}$$

where Δx_r denotes the cell volume divided by cell area parallel to the wall, which arises from integrating over boundary cell and applying boundary condition and not directly from volume/area ratio, c_i the gas composition of produced gas in mole fraction, and the ρ terms the densities in the wall and the bed, respectively. It is this change in the density from that of the wall and the bed which produces the various species near the wall. The values of these bed and wall densities should be chosen - in some cases artificial density values - so as to yield appropriate gas evolution at the wall region.

APPENDIX E. ANALYTIC SOLUTION FOR RADIATIVE TRANSPORT AT BED EXIT

The case of zero radiant loss at the bed exit has already been treated in the section on the verification (Sec. IV, case 4). Here we present a closed-form solution for a one-dimensional flow with radiant heat loss at the bed exit plane. To recapitulate, we have:

$$k\, d^2T/dy^2 - (CUc_g)dT/dy - (hA_s/A_c)(T - T_w) = 0 \qquad (37)$$

where the term h denotes the heat-transfer coefficient (taken to be a constant here), A_s/A_c the ratio of the bed surface area to the cross-sectional area of the bed, and the other terms have their usual meanings.

with the boundary conditions

$$\text{inlet } (y = 0) ; \quad Cc_gUT_{inj} = Cc_gUT - kdT/dy ;$$

$$\text{exit } (y = L) ; \quad - kdT/dy = S(T^4 - T^4_{ambient}).$$

where the term S is a function denoting combination of the radiation shape factor, the emissivity of the flowing gas, and the Stefan-Boltzmann constant.

The analytic solution to Eq.(37) is :

$$T(y) - T_w = A \exp(O_2 y) + B \exp(-O_3 y) \qquad (E.1)$$

where $p = Cc_gU/k$; $q = (hA_p/kA_c)$; $O_1=(p^2+4q)^{1/2}$;

and $O_2=(O_1+p)/?$; $O_3=(O_1-p)/2.$

The coefficients A and B can be determined from the boundary conditions.

The condition at y=0 yields

$$Z_1 A + Z_2 B = Z_3 \qquad (E.2)$$

where $Z_1 = G c_g - k Q_2$; $Z_2 = G c_g + k Q_3$;

$Z_3 = G c_g (T_{inj} - T_w)$.

From the condition at y=L we obtain

$$S [(Q_4 A + Q_5 B + T_w)^4 - T_{amb}^4] = - Z_4 A + Z_5 B \qquad (E.3)$$

where $S = \sigma \varepsilon F_s$; $Z_4 = k Q_2 Q_4$; $Z_5 = k Q_3 Q_5$.

$Q_4 = \exp(Q_2)$; and $Q_5 = \exp(-Q_3)$.

We thus have two equations and two unknowns A and B.

For A: from Eq.(E.2)

$$A = (Z_3 - Z_2 B)/Z_1 \qquad (E.4)$$

Determination of B is more complicated due to the quartic nature of Eq.(E.3). Combining Eqs.(E.3) and (E.4), and performing a series of algebraic manipulations, we obtain

$$B^4+4Z_{12}B^3+6Z_{12}B^2+(4Z_{12}^2-Z_{13})B+(Z_{12}^4-Z_{14})=0 \qquad (E.5)$$

where $Z_6 = Z_4/(Q_4^4 S)$; $Z_7 = Z_5/(Q_4^4 S)$;

$Z_8 = Q_5/Q_4 - Z_2/Z_1$; $Z_9 = Z_3/Z_1 + T_w/Q_4$;

$Z_{10} = Z_7 + Z_2 Z_6/Z_1$; $Z_{11} = (T_w/Q_4)^4 - Z_3 Z_6/Z_1$;

$Z_{12} = Z_9/Z_8$; $Z_{13} = Z_{10}/(Z_8)^4$;

$Z_{14} = Z_{11}/(Z_8)^4$

There are four roots for B ; since we do not know a priori which root is the physically relevent one, we list all four solutions here :

$$B_1=-Z_{12}-\{-S_1-S_2-S_3\} \; ; \; B_2=-Z_{12}-\{-S_1+S_2+S_3\}$$

$$B_3=-Z_{12}-\{\ S_1-S_2+S_3\} \; ; \; B_4=-Z_{12}-\{\ S_1+S_2-S_3\}$$

where $S_1=W_1^{1/2}$; $S_2=W_2^{1/2}$; $S_3=W_3^{1/2}$.

The terms W_1, etc., are in turn obtained to be :

$$W_1 = \quad M + N \; ;$$
$$W_2 = -(M + N)/2 + i(3)^{1/2}(M - N)/2 \; ;$$
$$W_3 = -(M + N)/2 - i(3)^{1/2}(M - N)/2 \; ;$$

$$M = \{-E_a/2 + (E_c)^{1/2}\}^{1/3} \; ; \; N = \{-E_a/2 - (E_c)^{1/2}\}^{1/3};$$

and

$$E_a = -Z_{13}^2/64 \; ; \quad E_b = -(Z_{12}\ Z_{13} - Z_{14})/4 \; .$$

$$E_c=(E_b/3)^3+(E_a/2)^2 \; ;$$

For $E_c < 0$, an alternative expression for the three roots are :

$$W_1 = (- \text{ or } +)\ 2\ (-E_c/3)^{1/2} \cos\ (\theta/3) \; ;$$
$$W_2 = (- \text{ or } +)\ 2\ (-E_c/3)^{1/2} \cos\ (\theta/3 +120) \; ;$$
$$W_3 = (- \text{ or } +)\ 2\ (-E_c/3)^{1/2} \cos\ (\theta/3 +240) \; ;$$

where

θ = arc cos $([E^a/4\}/\{-E_c^3/27\}]^{1/2})$ and the - or + sign is for $E_a \to 0$, or $E_a \to 0$, respectively.

As an example, for the conditions used in the verification runs (with ambient temperature of 600 K, emissivity of 0.7 and shape factor of unity as additional conditions), we obtain: $A = -0.078$; $B = 72.89$.

As stated in the main text, the GSF computer results agree very well with this analytic solution.

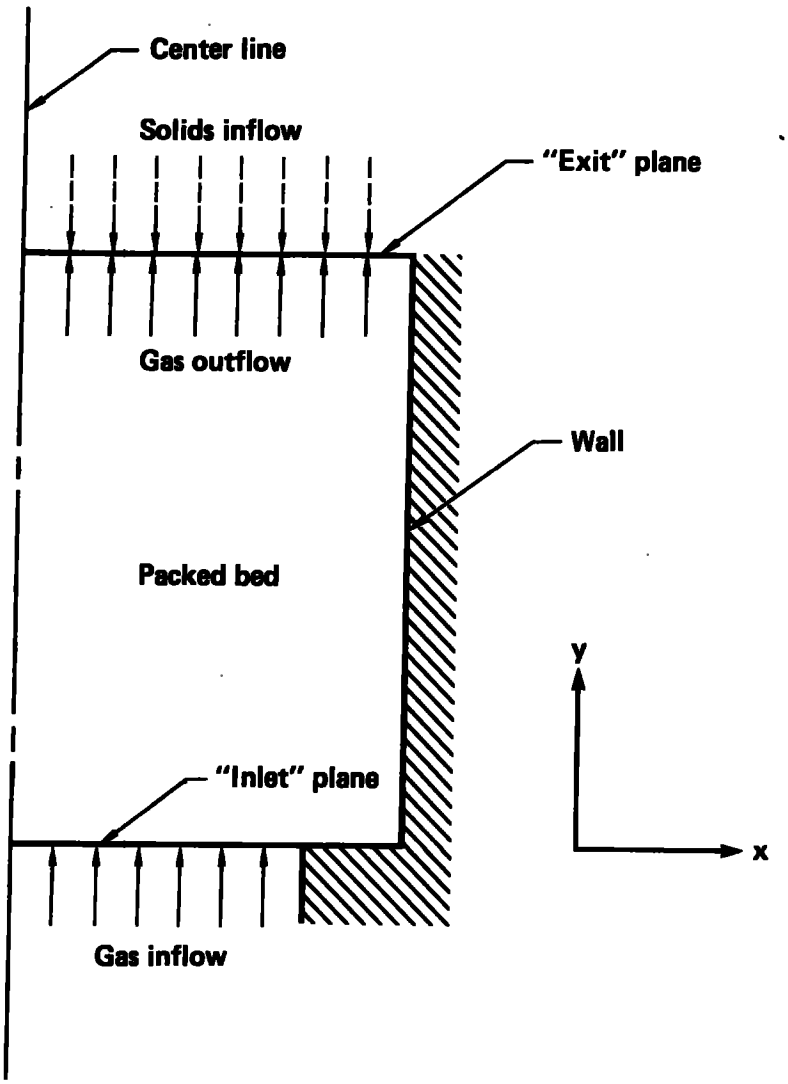

Figure 1. Packed Bed Geometry (Schematic).

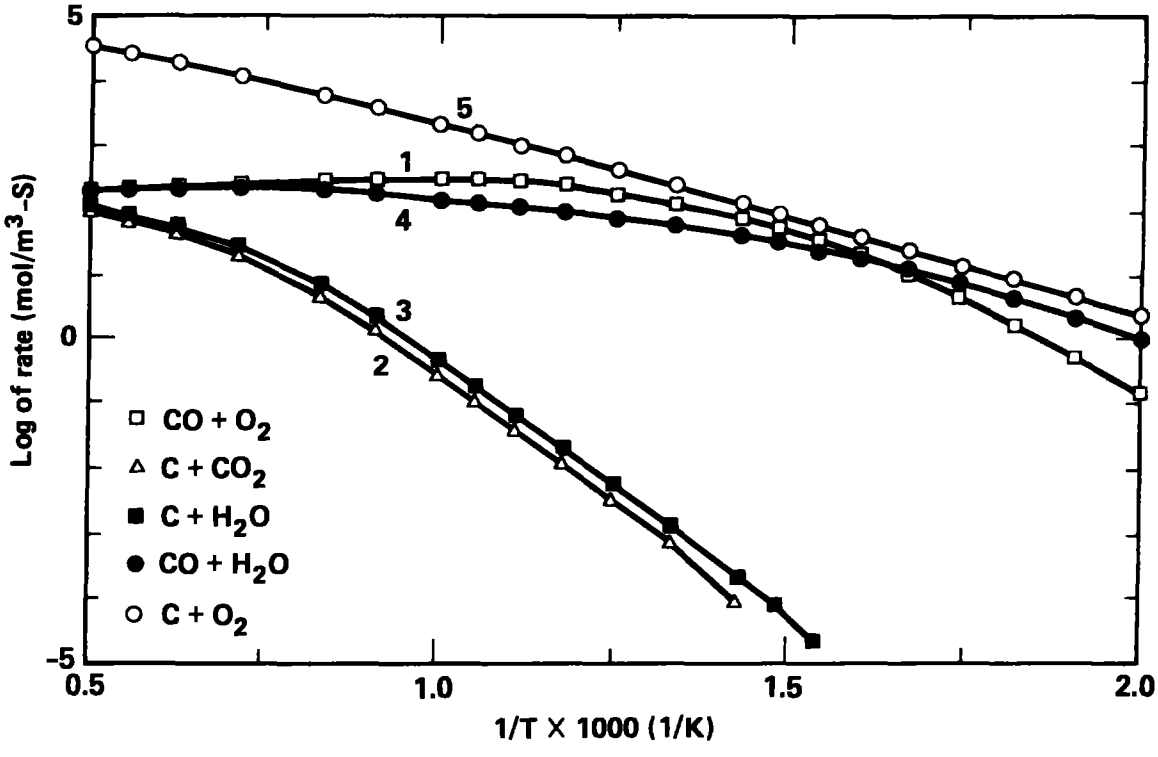

Figure 2. Reaction Rates in Packed Beds for SP and AS Models. Reaction 1: $CO+O_2$ -> CO_2; 2: $C+CO_2$ <-> $2CO$; 3: $C+H_2O$ <-> $CO+H_2$; 4: $CO+H_2O$ <-> CO_2+H_2; 5: $C+O_2$ -> $CO+CO_2$; d_p=0.025 m; G=1 mol/m_2-s.

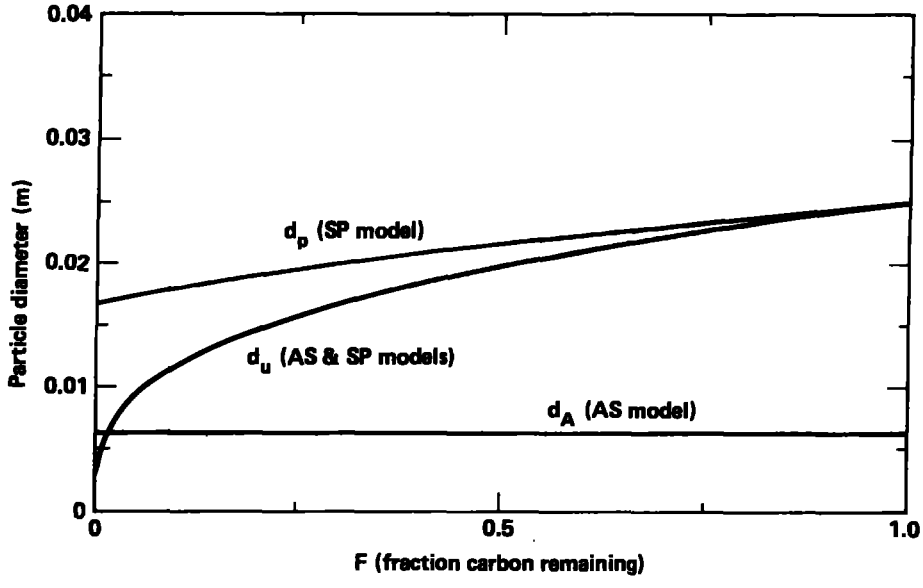

Figure 3. Particle Size Changes for SP and AS Models (Assuming Constant Bed Density).

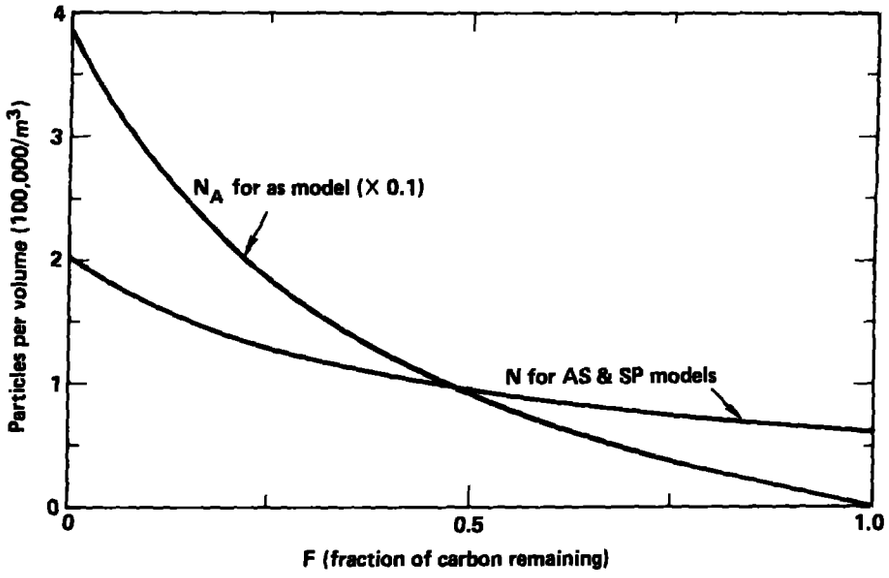

Figure 4. Particle Number Density Changes for SP and AS Models (Assuming Constant Bed Density).

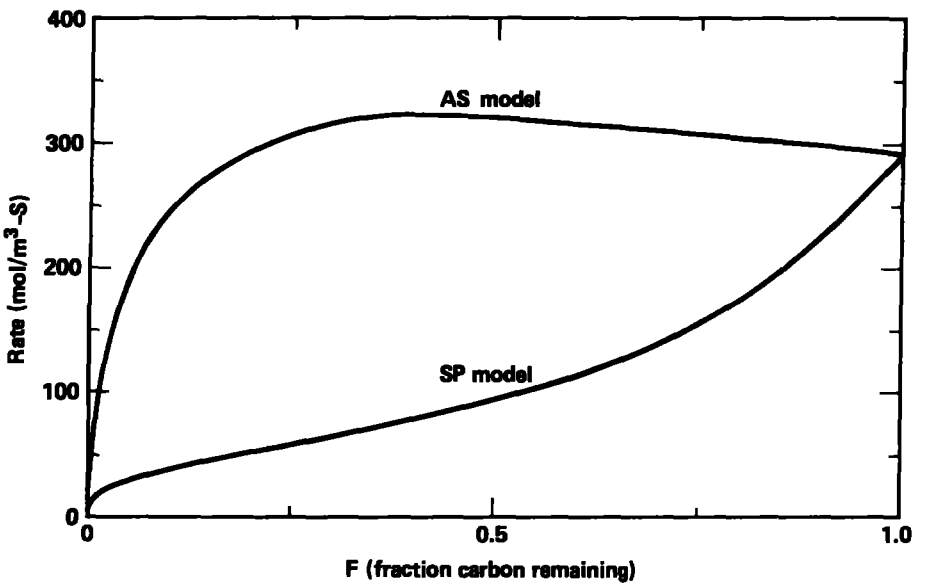

Figure 5. Effect of SP and AS Models on Carbon-Oxidation Rates.

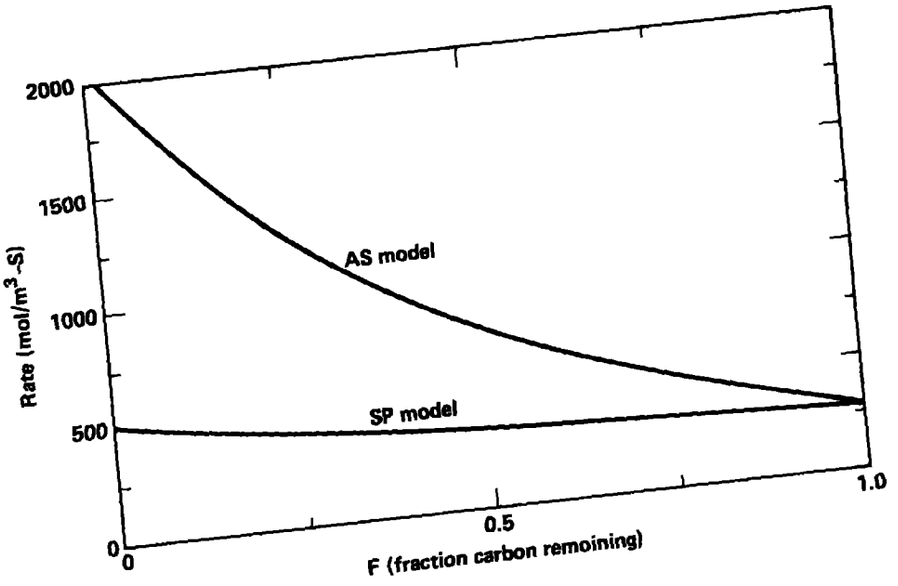

Figure 6. Effect of SP and AS Models on Water-Gas-Shift Rates.

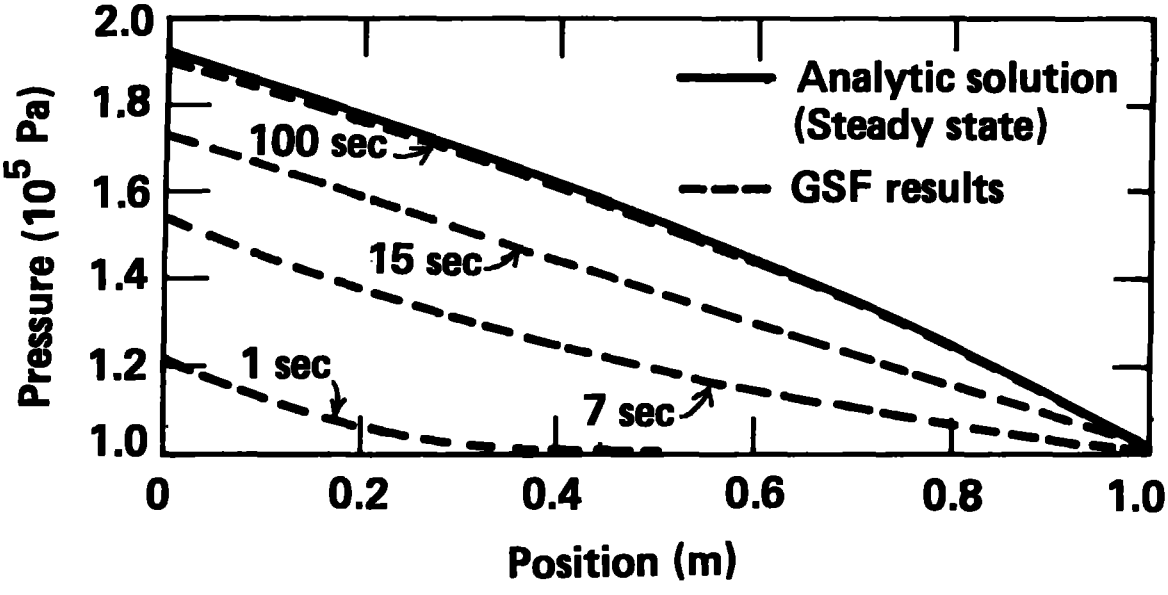

Figure 7. Comparison between Analytic Solution and GSF Calculations for One-dimensional Steady Flow inside a Packed Bed (Case 1).

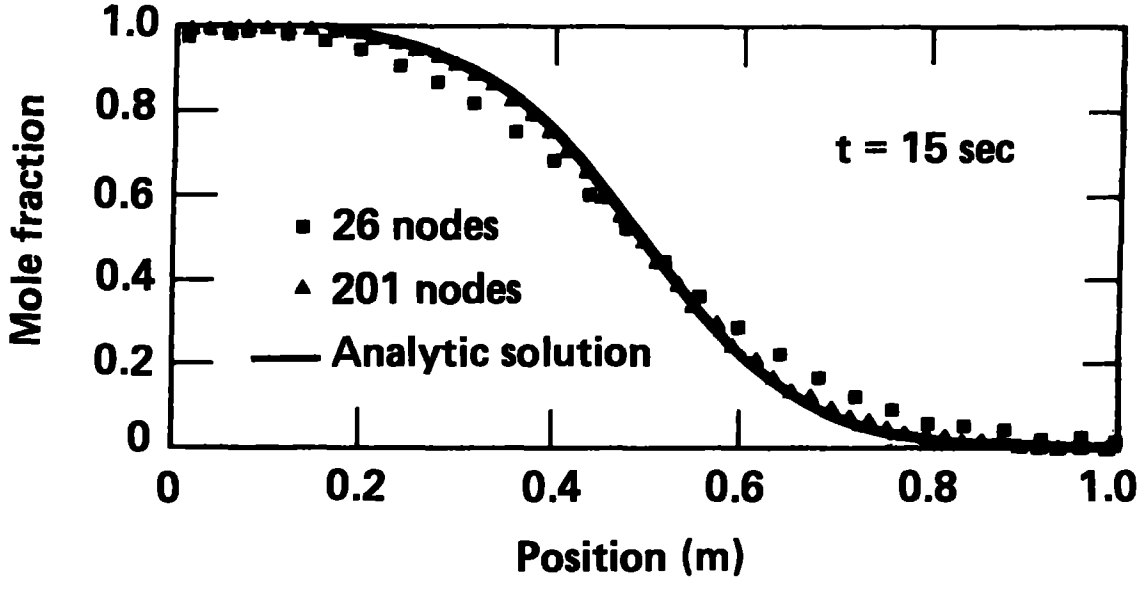

Figure 8. Comparison between Analytic Solution and GSF Calculations for One-dimensional Concentration Wave inside a Packed Bed (Case 2: t=15 sec).

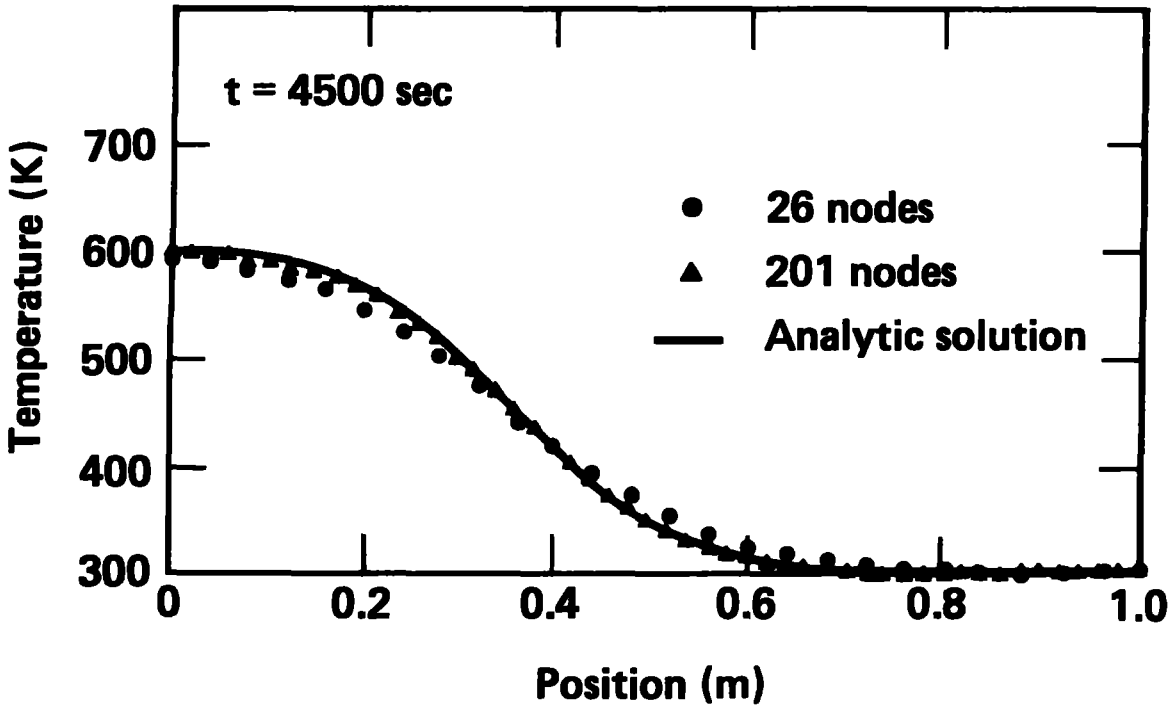

Figure 9. Comparison between Analytic Solution and GSF Calculations for One-dimensional Thermal Wave inside a Packed Bed (Case 3: t=4500 sec).

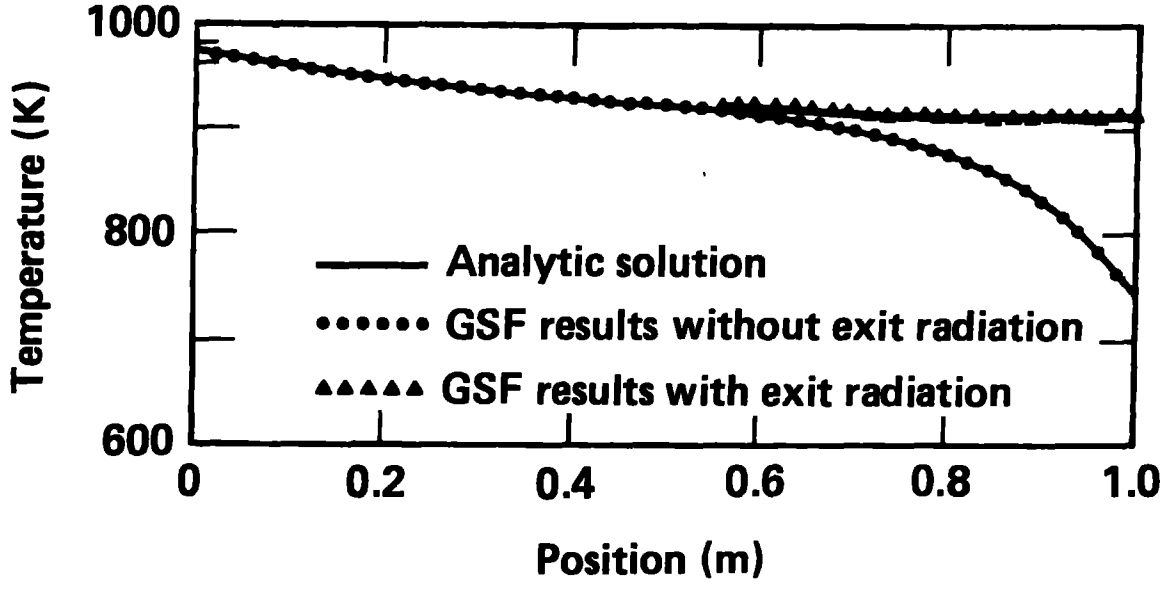

Figure 10. Comparison between Analytic Solution and GSF Calculations for One-dimensional Flow with Wall Heat Transfer inside a Packed Bed : with and without Radiation at Exit. (Case 4.)

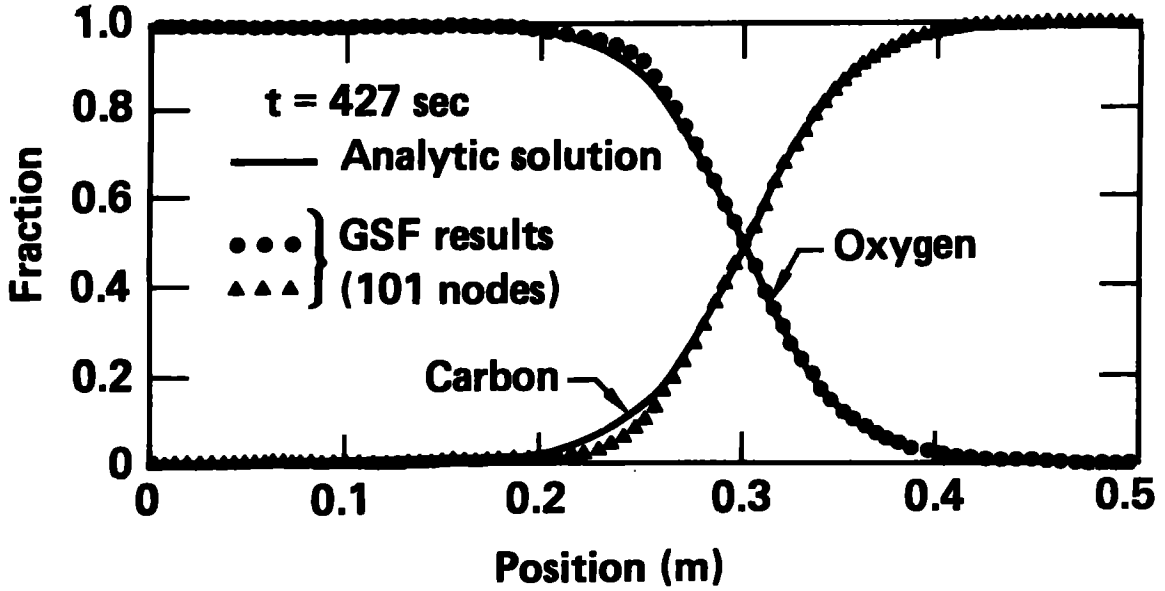

Figure 11. Comparison between Analytic Solution and GSF Calculations for Gas and Solid Distributions for a One-dimensional Catalytic Regeneration Flow (Case 5: t=427 sec).

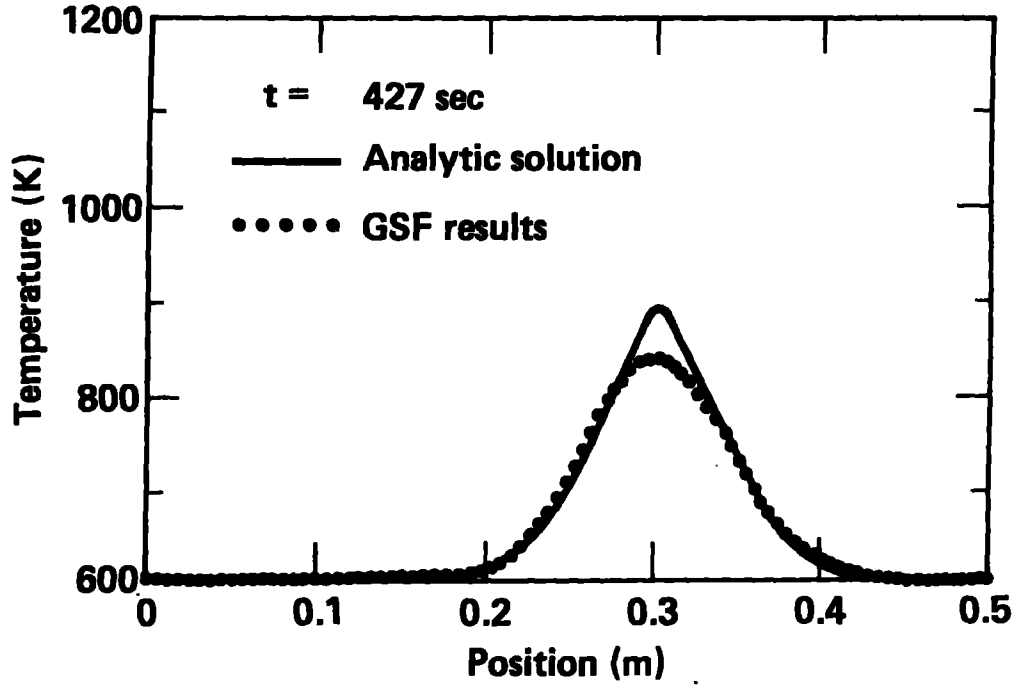

Figure 12. Comparison between Analytic Solution and GSF Calculations for Temperature Distribution in the Reaction Zone of a One-dimensional Catalytic Regeneration Flow (Case 5: t=427 sec).

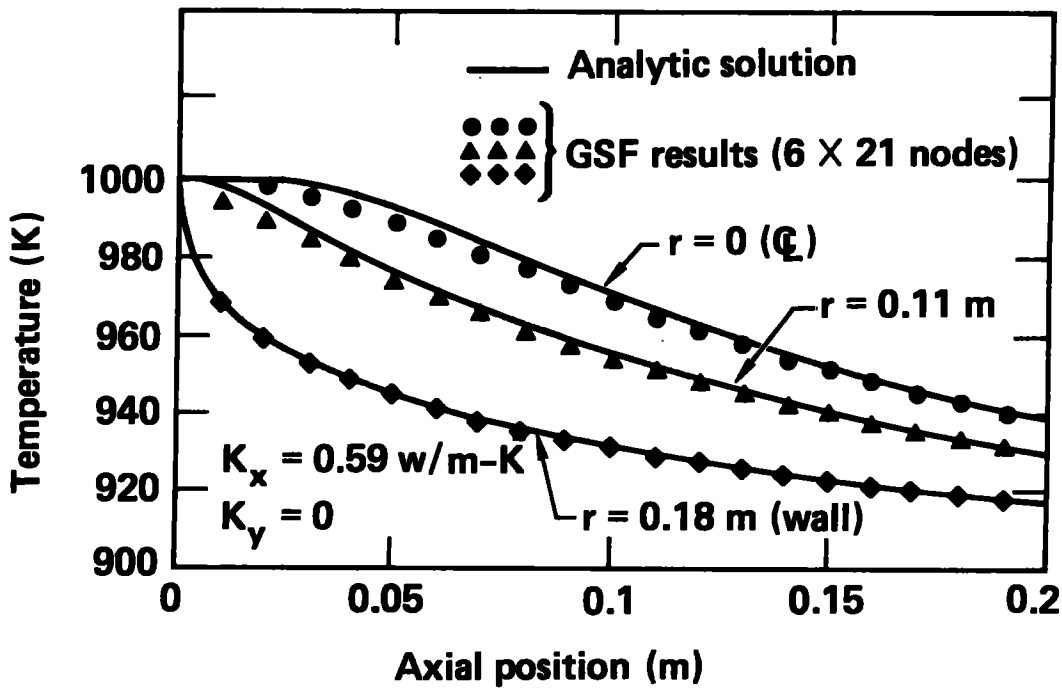

Figure 13. Comparison between Analytic Solution and GSF Calculations for Temperature Distribution in a Non-isotropic Bed for Two-dimensional Flow with Wall Heat Transfer (Case 6).

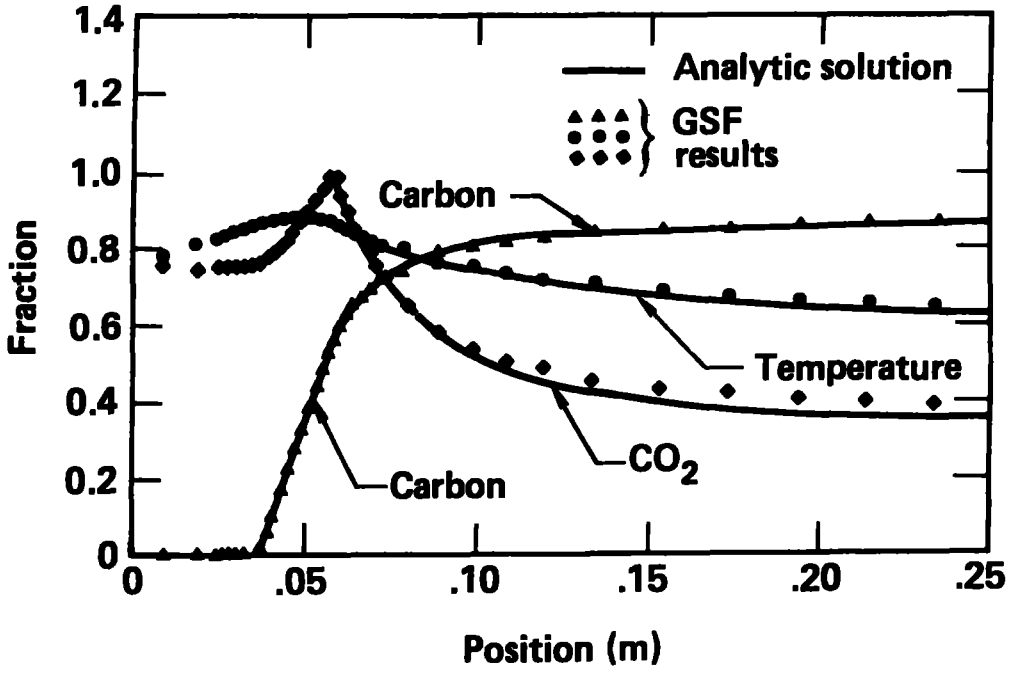

Figure 14. Comparisons between Analytic Solution and GSF Calculations for One-dimensional Gasification Flow inside a Packed Bed (Case 7).

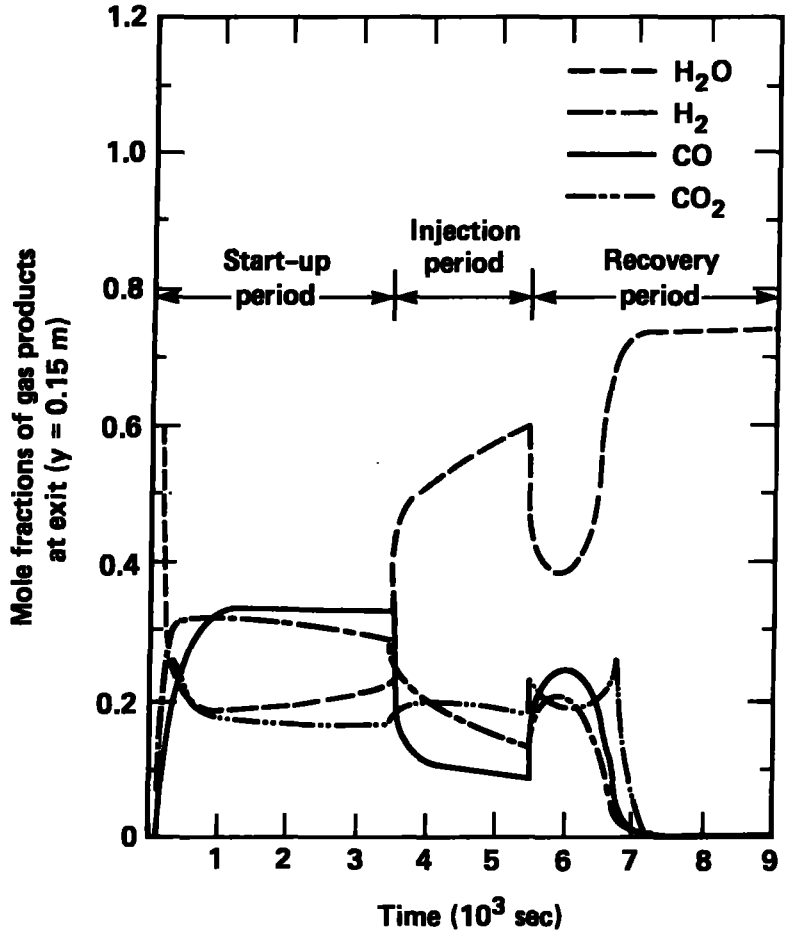

Figure 15. Product Gas Changes during Gasification of a One-dimensional Packed Bed with Mid-point Water Injection.

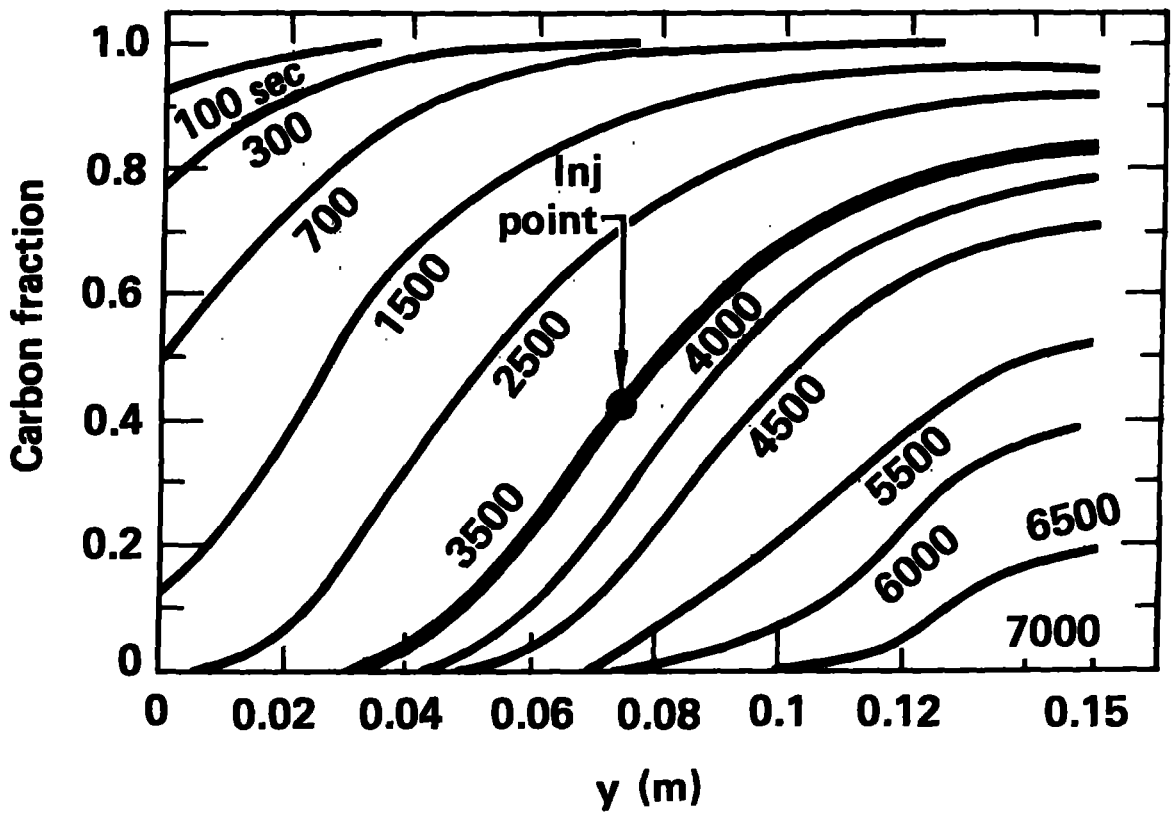

Figure 16. Changes in Carbon Fraction during Gasification of a One-dimensional Packed Bed with Mid-point Water Injection.

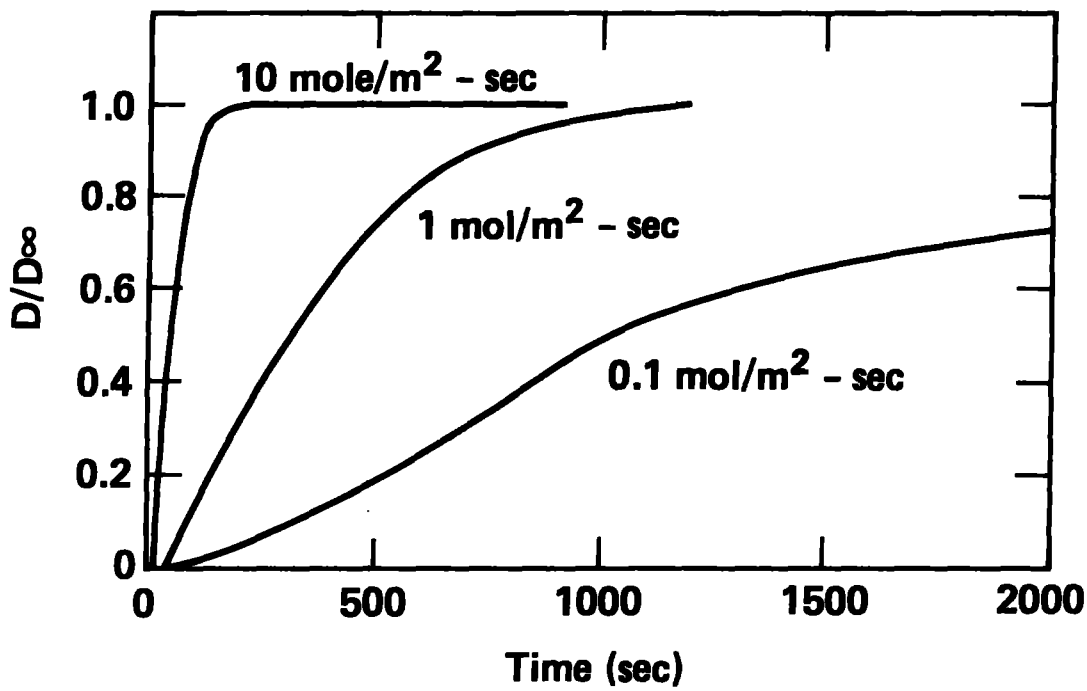

Figure 17. Drying-rate History for Three Flow Rates (Wall-Drying Problem).

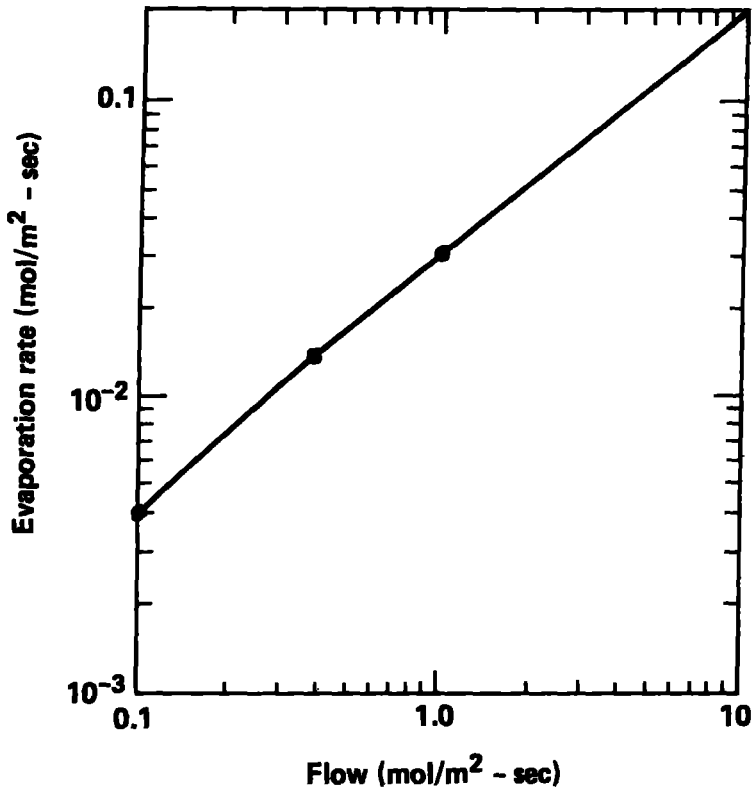

Figure 18. Drying Rate vs. Flow Rate (Wall-Drying Problem).

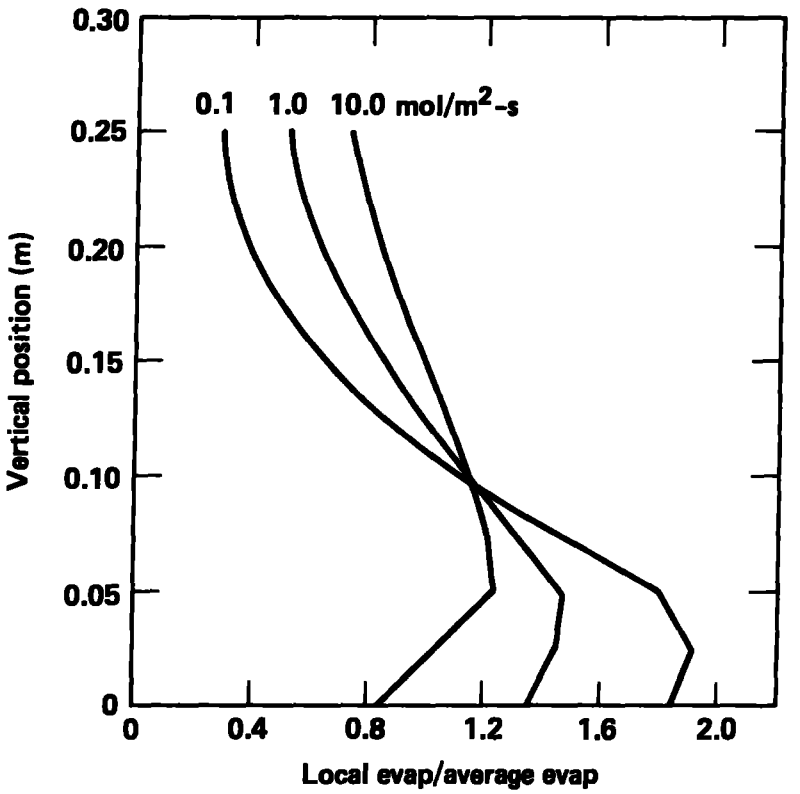

Figure 19. Distribution of Drying Rates along Bed for Three Flow Rates (Wall-Drying Problem).

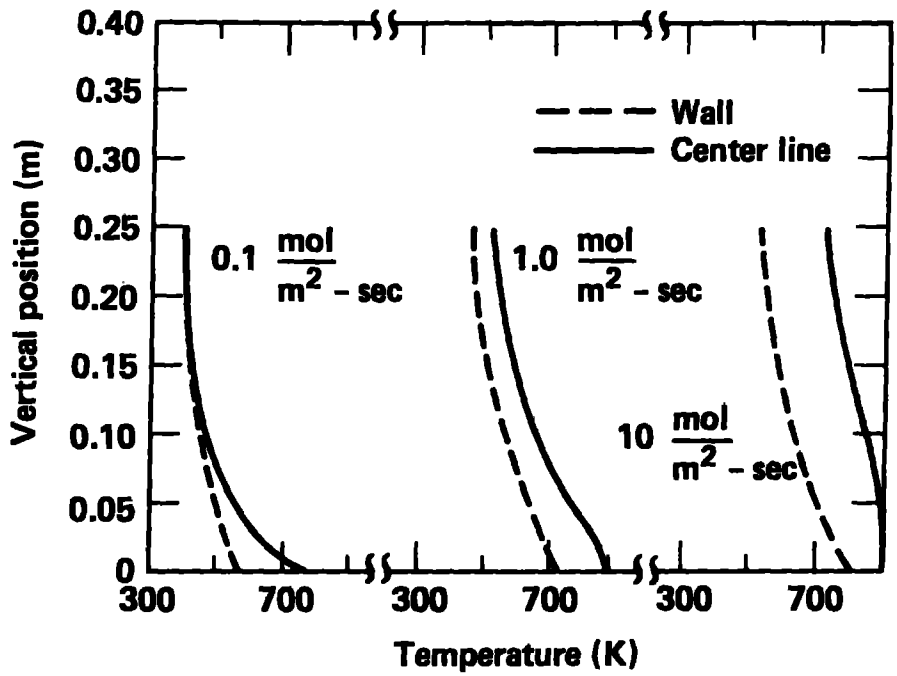

Figure 20. Temperature Profiles at Wall and Centerline for Three Flow Rates (Wall-Drying Problem).

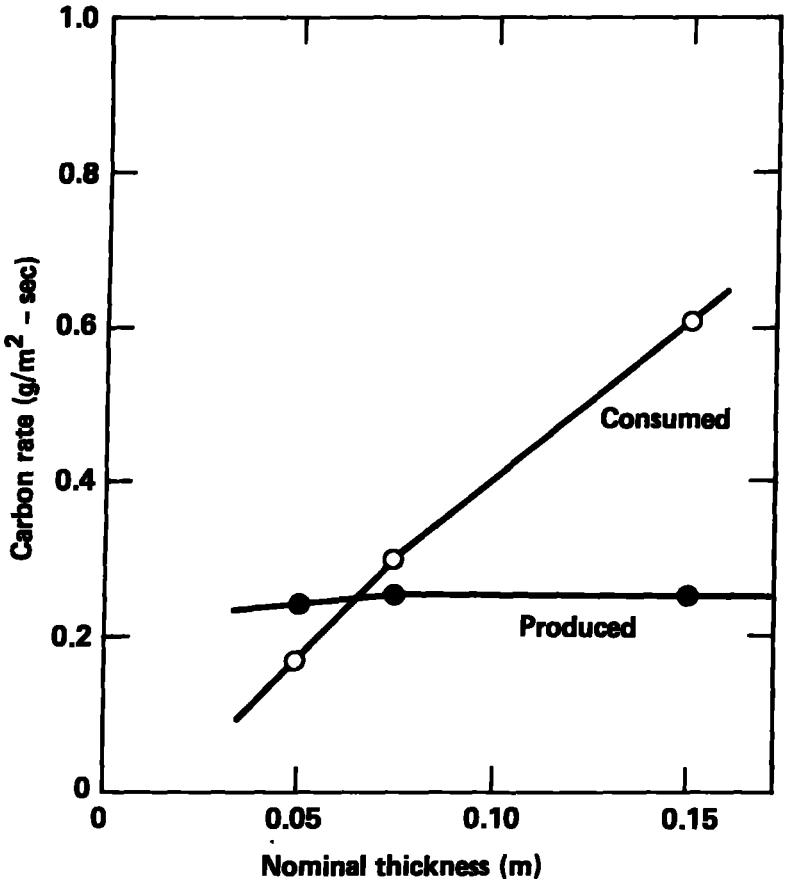

Figure 21. Carbon Production Rate vs. Wall Char-layer Thickness (Wall Regression Problem).

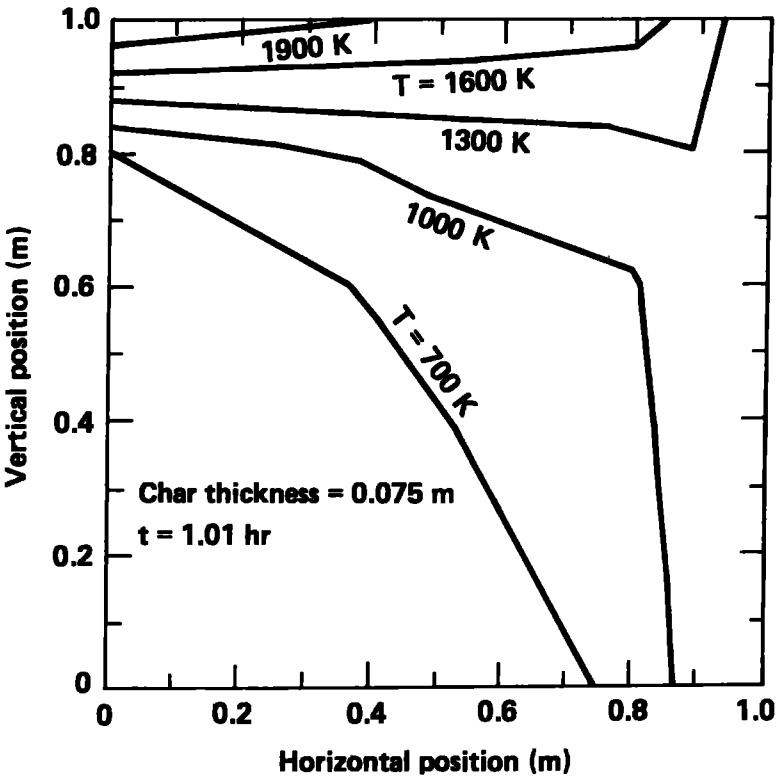

Figure 22. Temperature Distribution inside a Packed Bed at t=1.01 hr (Wall Regression Problem).

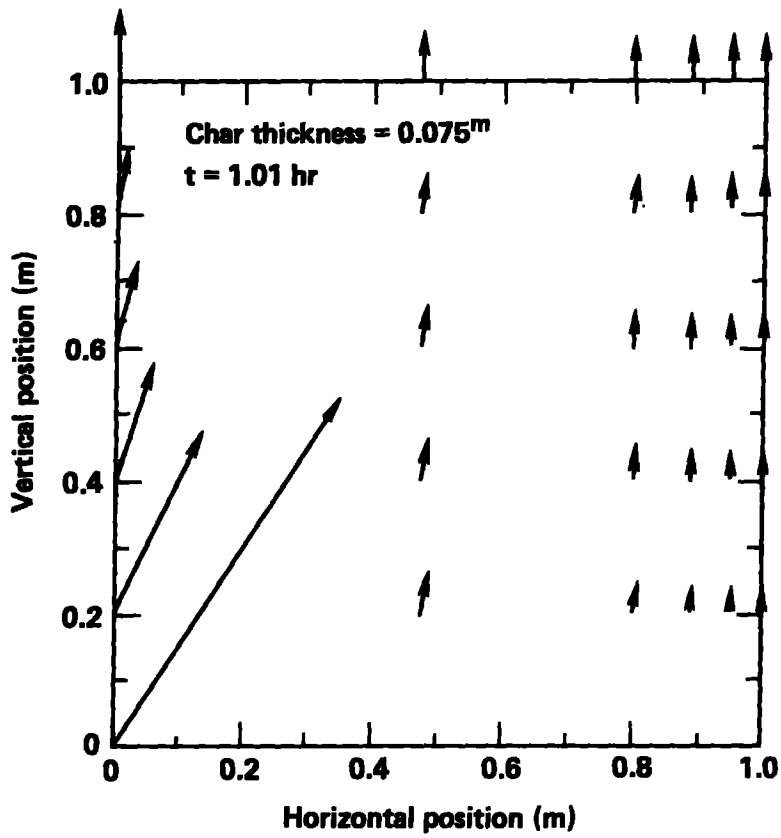

Figure 23. Local Gas Flux Distribution inside a Packed Bed at t=1.01 hr (Wall Regression Problem).

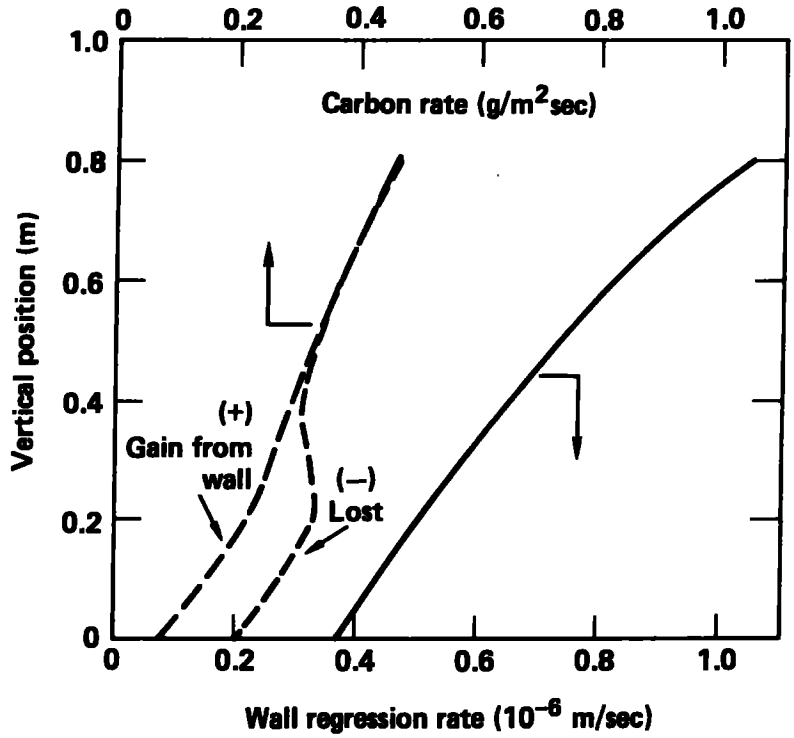

Figure 24. Local Carbon and Wall-regression Rates along Vertical Position in the Bed (Wall Regression Problem).

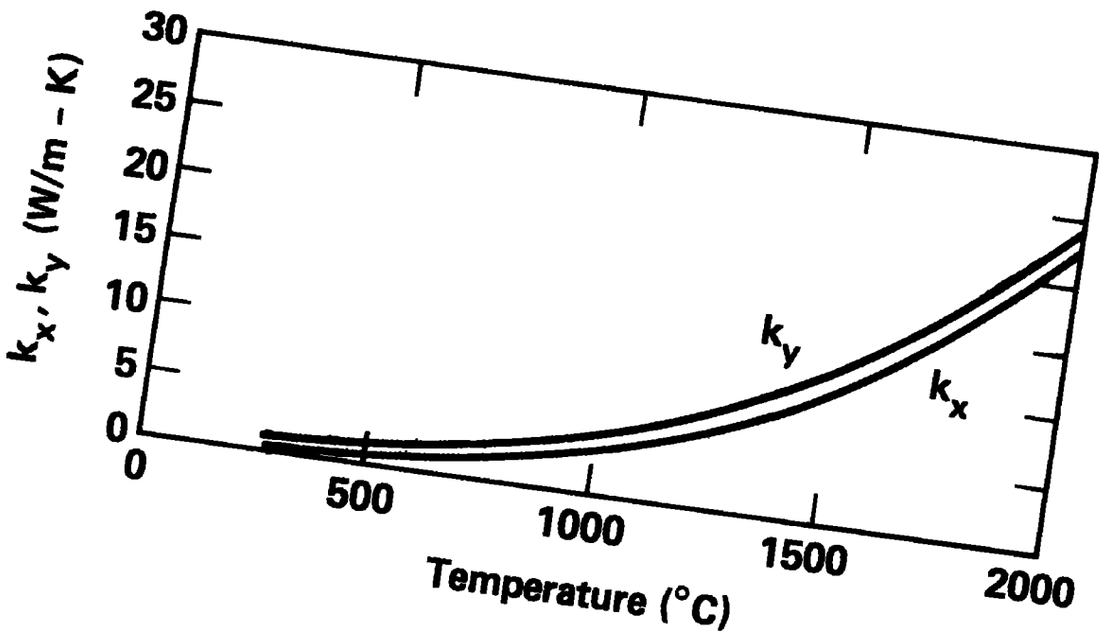

Figure B.1. Variations of Effective Thermal-Dispersion Coefficients with Temperature.

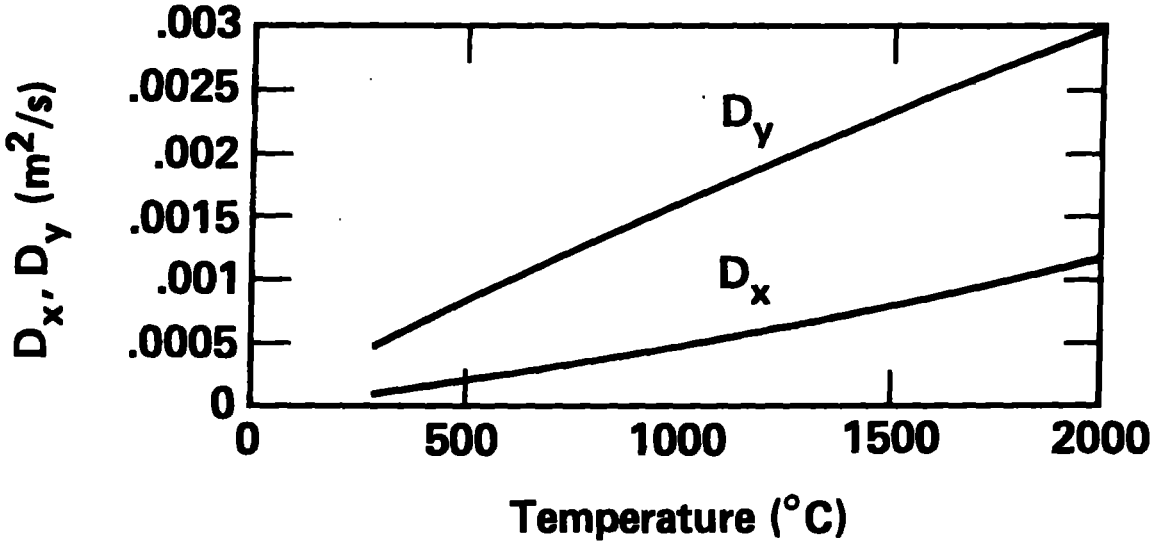

Figure B.2. Variations of Effective Mass-Dispersion Coefficients with Temperature.

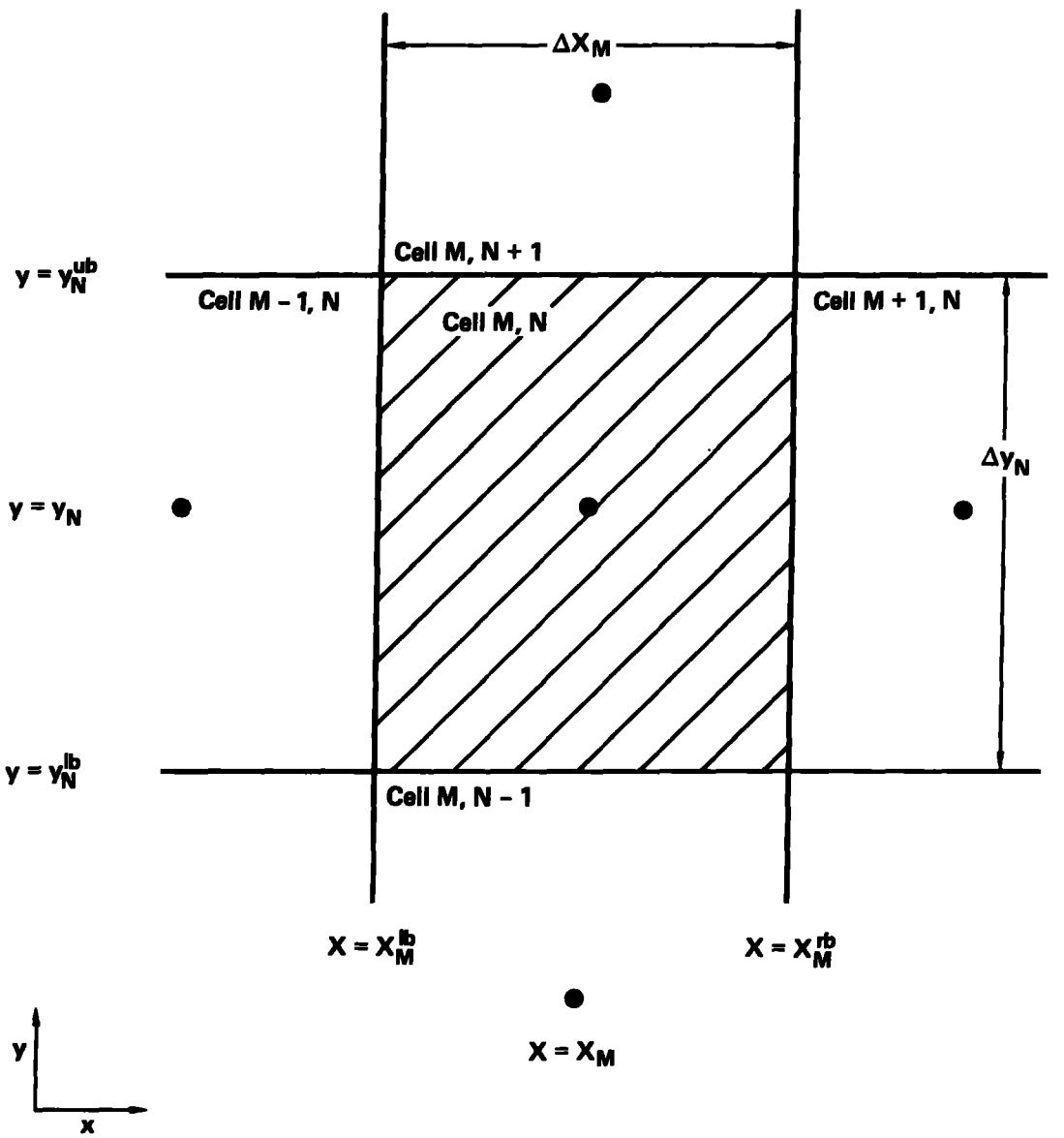

Figure C.1. Two-dimensional Mesh Geometry.

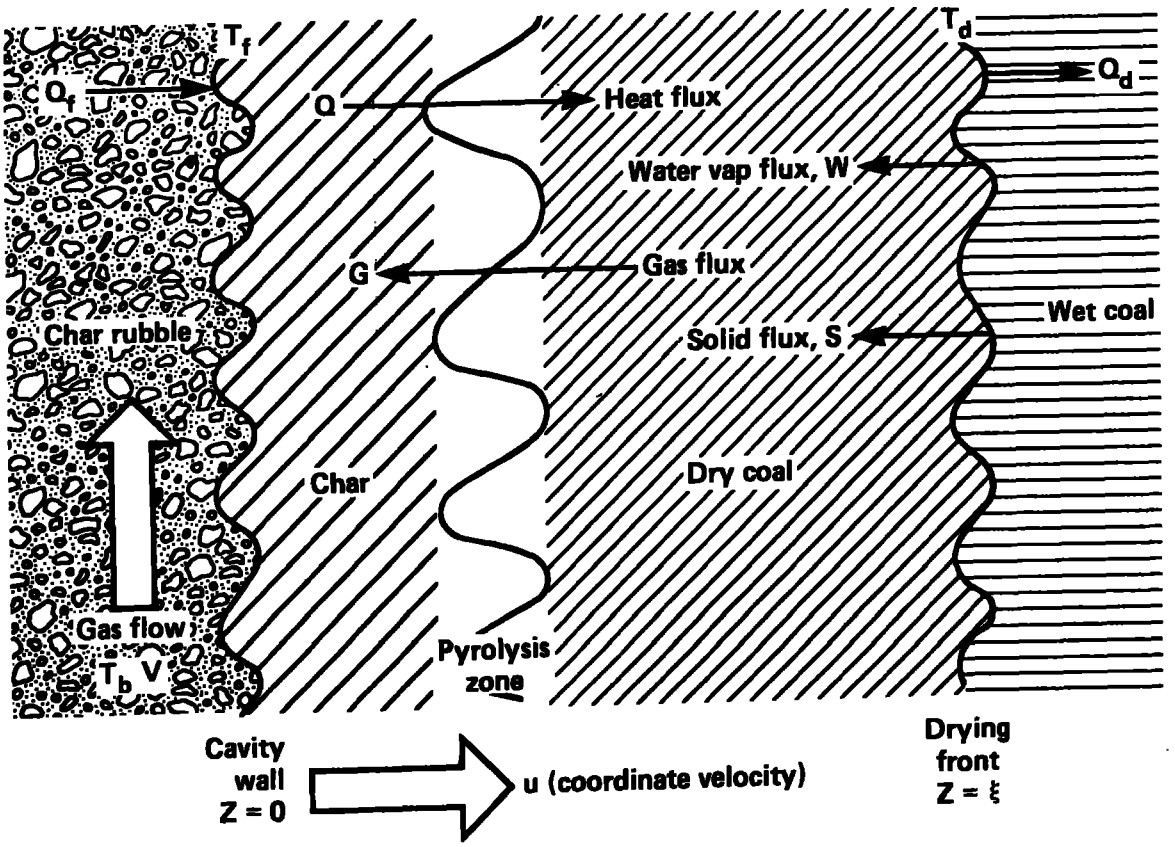

Figure D.1. Physico-chemical Processes at UCG Cavity Wall.